

521591 / N-47  
121088  
p. 46

NASA  
Technical  
Paper  
3230

September 1992

# Inertial Oscillation of a Vertical Rotating Draft With Application to a Supercell Storm

Robert C. Costen  
and Larry V. Stock

(NASA-TP-3230) INERTIAL  
OSCILLATION OF A VERTICAL ROTATING  
DRAFT WITH APPLICATION TO A  
SUPERCCELL STORM (NASA) 46 p

N92-33482  
Unclas  
H1/47 0121088



**NASA**  
**Technical**  
**Paper**  
**3230**

1992

# Inertial Oscillation of a Vertical Rotating Draft With Application to a Supercell Storm

Robert C. Costen  
*Langley Research Center*  
*Hampton, Virginia*

Larry V. Stock  
*Hampton University*  
*Hampton, Virginia*

**NASA**  
National Aeronautics and  
Space Administration  
Office of Management  
Scientific and Technical  
Information Program

Contents

1. Introduction . . . . .	1
2. Model Description . . . . .	2
2.1. Coordinate Frame . . . . .	2
2.2. Storm Idealizations . . . . .	2
3. Inner Solution . . . . .	4
3.1. Velocity Field . . . . .	4
3.2. Momentum Equation . . . . .	4
3.3. Second-Order Partial Derivatives . . . . .	5
3.4. Nonlinear Harmonic Equations . . . . .	6
3.5. Pressure Field . . . . .	6
3.6. Thermodynamic Energy Equation . . . . .	7
4. Numerical Integration and Supercell Solution . . . . .	8
4.1. Inertial Oscillation of $\zeta$ and $D$ . . . . .	8
4.2. Buoyancy . . . . .	9
4.3. Core Radius $a$ and Angular Displacement $\theta$ . . . . .	9
4.4. Diabatic Heating and Moisture Influx . . . . .	10
4.5. Constant of the Motion and Froude Number . . . . .	10
4.6. Horizontal Vorticity Components $\xi$ and $\eta$ . . . . .	11
4.7. Translation $\dot{x}_c, \dot{y}_c$ and Track $x_c, y_c$ . . . . .	11
5. Physics of Inertial Oscillation . . . . .	13
5.1. Inertial Flow . . . . .	13
5.2. Contraction and Cyclonic Spin-Up . . . . .	13
5.3. Increased Contraction and Cyclonic Spin-Up . . . . .	14
5.4. Singular Point . . . . .	14
5.5. Anticyclonic Spin-Up . . . . .	14
5.6. Steady-State Anticyclonic Rankine Vortex . . . . .	15
6. Implications for Numerical Simulations . . . . .	15
7. Concluding Remarks . . . . .	15
Appendix A—Basic Rotating Draft That Oscillates But Does Not Translate . . . . .	17
Appendix B—Physical Interpretation of Translation Formulas . . . . .	22
Appendix C—Further Properties of Inertial Oscillation . . . . .	23
References . . . . .	25

## Symbols

$A$	arbitrary scalar field or Cartesian component of vector field
$a$	core radius, m
$B$	normalized density deficit or "buoyancy" (eq. (1c))
$b$	height of surface layer above mean sea level, m
$C$	arbitrary integration function of $t$ (eq. (A7))
$c_p$	specific heat at constant pressure, $1004 \text{ J}\cdot\text{kg}^{-1}\cdot\text{K}^{-1}$
$D$	velocity divergence, $\text{s}^{-1}$
$F$	Froude number
$f_B$	buoyant force density, $\text{N}\cdot\text{m}^{-3}$
$g$	acceleration of gravity, $9.81 \text{ m}\cdot\text{s}^{-2}$
$h$	height of upper layer above mean sea level, m
KE	kinetic energy density, $\text{kg}\cdot\text{m}^{-1}\cdot\text{s}^{-2}$
$L_z$	$z$ -component of angular momentum density about centerline, $\text{kg}\cdot\text{m}^{-1}\cdot\text{s}^{-1}$
$\dot{M}$	net upward mass flux, $\text{kg}\cdot\text{s}^{-1}$
$\dot{M}_v$	net water vapor influx, $\text{g}\cdot\text{s}^{-1}$
MDT	mountain daylight time
$p$	pressure, Pa
$\dot{Q}$	total diabatic heating of core, W
$\dot{q}$	diabatic heating per unit volume, $\text{W}\cdot\text{m}^{-3}$
$R$	gas constant for dry air, $287 \text{ J}\cdot\text{kg}^{-1}\cdot\text{K}^{-1}$
$R_i$	inertial radius projected on horizontal plane (eq.(20)), m
Ro	Rossby number
$r$	radius in cylindrical coordinate frame (fig. 1(b)), m
$\dot{\mathbf{r}}_c$	translational velocity of rotating draft centerline $(\dot{x}_c, \dot{y}_c, 0)$ , $\text{m}\cdot\text{s}^{-1}$
$S$	supply
$T$	temperature, K
$t$	time, s
$U_b, V_b$	constants that represent uniform part of horizontal flow at base of core
$u, v, w$	Cartesian components of fluid velocity, $\text{m}\cdot\text{s}^{-1}$
$\mathbf{V}_b$	constant components of horizontal velocity, $(U_b, V_b, 0)$ , $\text{m}\cdot\text{s}^{-1}$
$\mathbf{v}$	fluid velocity, $\text{m}\cdot\text{s}^{-1}$
$v_i$	inertial speed, (eq. (20)), $\text{m}\cdot\text{s}^{-1}$
$v_r, v_\theta, v_z$	cylindrical components of fluid velocity, $\text{m}\cdot\text{s}^{-1}$

$v^a(\zeta, D)$	constant of the motion (eq. (18a)), $\text{m}\cdot\text{s}^{-1}$
$X, Y, Z$	relative Cartesian coordinates $(x - x_c, y - y_c, z - b)$ , m
$x, y, z$	Cartesian coordinates (fig. 1(a)), m
$x_c, y_c$	Cartesian coordinates of rotating draft centerline on horizontal plane (fig. 2), m
$\Gamma$	vortex circulation of rotating draft (see sec. 4.3), $\text{m}^2\cdot\text{s}^{-1}$
$\epsilon$	inverse of density scale height, $\text{m}^{-1}$
$\theta$	angular displacement of core fluid (eq. (4)), rad
$\lambda$	east longitude, rad
$\xi, \eta, \zeta$	Cartesian components of vorticity, $\text{s}^{-1}$
$\rho$	air density, $\text{kg}\cdot\text{m}^{-3}$
$\rho^o(a)$	outer density at radius $a$ and height $z$ (eq. (1a)), $\text{kg}\cdot\text{m}^{-3}$
$\rho_b^o$	constant outer density at radius $a$ and height $b$ (fig. 2), $\text{kg}\cdot\text{m}^{-3}$
$\dot{\rho}_v$	condensation rate of water vapor density, $\text{g}\cdot\text{s}^{-1}\cdot\text{m}^{-3}$
$\tau$	period of inertial oscillation (eq. (14)), s
$\Phi$	geopotential, $\text{m}^2\cdot\text{s}^{-2}$
$\phi$	latitude, rad
$\Omega$	Earth's angular velocity, $\text{rad}\cdot\text{s}^{-1}$
$\omega$	vorticity, $\text{s}^{-1}$
$0, \Omega_y, \Omega_z$	Cartesian components of Earth's angular velocity, $\text{rad}\cdot\text{s}^{-1}$
Subscript:	
$H$	horizontal
Superscript:	
$o$	region of middle troposphere outside core

A dot over a symbol denotes a time derivative; a carat over a symbol denotes a unit vector; vertical bars around a symbol denote an absolute value; a boldface symbol denotes a vector.

## Abstract

*An analytic model (“vertical rotating draft”), which includes the gross features of a supercell storm on an  $f$ -plane, undergoes an inertial oscillation that appears to have been overlooked in previous analytic and numerical models. The oscillation is nonlinear and consists of a long quiescent phase and a short intense phase. During the intense phase, the rotating draft has the following features of a supercell: the diameter of the core contracts as it spins up and expands as it spins down; if vertical wind shear is included, the track of the rotating draft turns to the right (an anticyclonic rotating draft turns to the left); this turning point is followed by a predominantly upward flow; and the horizontal pressure gradient is very small (a property of most tornadoless supercells). The rapid spin-up during the intense phase and the high Rossby numbers obtainable establish the ability of the Coriolis force to spin up single cyclonic or anticyclonic supercells by means of this inertial oscillation. This surprising result has implications for numerical supercell simulations, which generally do not rely on the Coriolis force as a source of rotation. The physics and mathematics of the inertial oscillation are given, and the solution is applied to a documented supercell.*

## 1. Introduction

Inertial oscillations are known to occur in the oceans. However, as Holton (ref. 1) states, “Pure inertial oscillations are apparently not of importance in the Earth’s atmosphere.” Our main objective is to present a new analytic model (vertical rotating draft) that exhibits an inertial oscillation in the middle troposphere. The model results from attempting to include (albeit very crudely) more of the gross features of a supercell storm than have been included in previous analytic models (refs. 2 through 8). (A supercell storm is a rotating thunderstorm that can generate tornadoes and hail.) These features are its net draft, rotation, vertical wind shear, divergence resulting from the expansion of rising air parcels, buoyancy, translation, and time dependence. The inertial oscillation occurs when the Coriolis force is also included.

Inertial oscillations appear to have been overlooked in the previous analytic models and in numerical simulations of supercells (refs. 9 through 13). This oscillation, which engages all features of the rotating draft, is described mathematically and physically. Other objectives are to apply the analytic solution to a documented supercell and to discuss its implications for the numerical simulations, which presently use other means than the Coriolis force to develop rotation.

The analytic model is defined in section 2. An inner solution and matching outer solution are given in appendix A for a *basic* rotating draft, one that oscillates but does not translate. A generalized inner solution, which includes translation but is not matched to the environmental flow (outer solution), is given in section 3. The analysis reduces to a set of nonlinear ordinary differential equations (ODE’s) for vorticity, divergence, core radius, translation. These ODE’s are numerically integrated forward in time and applied to a documented supercell in section 4. The inertial oscillation is described physically in section 5. Its implications for numerical simulations are discussed in section 6. The translational equations are interpreted physically in appendix B. Other features of the inertial oscillation are given in appendix C. These features include the effects of varying the peak Rossby number on the nonlinear waveforms of vorticity, divergence, and buoyancy; the inertial oscillation of an anticyclonic rotating draft; and an anticyclonic steady-state solution. A video supplement has been prepared and is available for purchase. A

request form and a description of the video are found at the back of this report. An earlier version of this video was presented at a conference (ref. 14).

## 2. Model Description

### 2.1. Coordinate Frame

The coordinate frame is a local tangential Cartesian frame whose origin is fixed at a point on the surface of the Earth (mean sea level) and whose  $x$ ,  $y$ , and  $z$  axes point eastward, northward, and upward, respectively, as shown in figure 1(a). (Cylindrical coordinates  $r, \theta, z$  are also used, as shown in fig. 1(b).) Although the  $x$  and  $y$  axes do not curve with the surface, this frame is adequate for describing tropospheric flows within a horizontal radius of about 60 km (ref. 15). This radius is large enough to contain the convective core of a supercell storm. However, the outer flow will exceed this radius. The use of spherical coordinates, although desirable, is beyond the scope of this paper.

In the Cartesian frame, the fluid velocity is denoted by  $\mathbf{v} = (u, v, w)$ , the vorticity by  $\boldsymbol{\omega} = (\xi, \eta, \zeta)$ , the divergence by  $D$ , and the angular velocity of the Earth by  $\boldsymbol{\Omega} = (0, \Omega_y, \Omega_z)$ . Although  $\Omega_y$  and  $\Omega_z$  are functions of  $y$ , we shall neglect this dependence and treat them as constants (“ $f$ -plane” approximation).

### 2.2. Storm Idealizations

Doppler radar measurements of a supercell storm by Miller, Tuttle, and Knight (ref. 16) show an inflow layer near the surface, an outflow layer near the top of the storm, a principal updraft that has its maximum at midheight, a secondary updraft, and a downdraft of lesser magnitude.

While retaining the gross features of this supercell, we greatly simplify its structure, as shown in figure 2, so that it can be treated analytically. The analysis is limited to the middle tropospheric layer between  $b$  and  $h$ , where  $b$  is the height of the surface layer and  $h$  is the height of the upper layer. Friction, heat conduction, and radiation are neglected in the middle layer, and tornadoes, which have large internal pressure drops, are assumed to be absent. Compatible solutions for the flows in the surface and upper layers are assumed to exist but are left for future work.

The core of the rotating draft is bounded laterally by a cylindrical interface of radius  $a(t)$ , which distinguishes the core from the outer region or environment. The jump conditions that apply at this interface are that the interface must move with the flow and that the pressure must be continuous across it. These jump conditions are enforced in the *basic* solution (appendix A), where they will determine the core radius  $a(t)$  and the core buoyancy  $B(t)$ . However, for the generalized rotating draft that translates (section 3), no attempt is made to match the inner solution to the outer flow by applying the jump conditions. Instead, we assume that such matching is always possible and that  $a(t)$  and  $B(t)$  are the same as in the basic, nontranslating solution.

As shown in figure 2, the location of the rotating draft centerline on the horizontal plane is given by  $(x_c(t), y_c(t))$ . The rotation is represented by a Rankine vortex of vorticity  $\zeta(t)$ , which is uniform inside the core and zero in the outer region. The density  $\rho$  is taken to decrease exponentially with height  $z$ . This idealization enables rising parcels of air to expand with divergence  $D(t)$ , which (like  $\zeta(t)$ ) is taken to be uniform inside the core and zero in the outer region. The core fluid is taken to be uniformly buoyant, as described by the normalized density deficit  $B(t)$  which will be simply called the “buoyancy.” Vertical wind shear is represented by the horizontal vorticity components  $\xi(t), \eta(t)$ , which are also taken to be uniform inside the core. When our crude analytic model is compared with an actual supercell, the fields  $\zeta(t), D(t)$ ,

$B(t)$  are identified with the instantaneous spatial averages in the core of the actual vorticity, divergence, buoyancy.

The density of the outer fluid at radius  $a$  is given by the idealization (ref. 6)

$$\rho^o(a) = \rho_b^o e^{-\epsilon Z} \quad (1a)$$

where  $Z \equiv z - b$ ,  $\rho_b^o$  is a constant that represents the density at level  $b$  just outside the core, and  $\epsilon$  is a constant that represents the inverse of the density scale height. (The fields outside the core ( $a \leq r$ ) will be distinguished by the superscript  $o$ .)

Inside the core, the density is prescribed by

$$\rho = \rho_b^o [1 - B(t)] e^{-\epsilon Z} \quad (1b)$$

where the buoyancy  $B \ll 1$  (a restriction that the supercell solution easily satisfies). Solving equation (1b) for  $B$  gives

$$B = \frac{\rho^o(a) - \rho}{\rho^o(a)} \quad (1c)$$

which confirms that  $B$  is the normalized density deficit in the core. The corresponding buoyant force density  $f_B$  (in  $\text{N}\cdot\text{m}^{-3}$ ) is given by

$$f_B = g[\rho^o(a) - \rho] = \rho g B \quad (1d)$$

where  $B^2$  has been neglected.

The continuity equation is given by

$$\frac{\partial \rho}{\partial t} + \mathbf{v} \cdot \nabla \rho + \rho D = 0 \quad (2a)$$

where  $D = \text{div } \mathbf{v}$ . By substituting the inner density (eq. (1b)) into equation (2a), we obtain in the core

$$D(t) = \epsilon w(t) \quad (2b)$$

where we have applied the Boussinesq approximation (ref. 17) in neglecting the  $\dot{B}$  term, whose smallness can afterwards be confirmed. In this approximation, we assume that the small density changes that correspond to the time-dependent buoyancy  $B(t)$  do not affect the divergence  $D(t)$ . By equation (2b), the draft velocity  $w$  is also spatially uniform in the core. Hence,  $D$  is a purely horizontal divergence given by

$$D = \frac{\partial u}{\partial x} + \frac{\partial v}{\partial y} \quad (2c)$$

As mentioned earlier, this divergence results from the expansion of ascending air parcels. The horizontal radial velocity resulting from  $D$  is proportional to the radius  $r$  inside the core and inversely proportional to  $r$  outside (like the rotational flow of the Rankine vortex) and it is uniformly distributed over the height of the middle layer ( $b < z < h$ ).

Also included in the core is a horizontal flow with vertical wind shear, which is represented by the constants  $U_b$  and  $V_b$  and the horizontal vorticity components  $\xi(t)$  and  $\eta(t)$ , as explained in section 3.

### 3. Inner Solution

#### 3.1. Velocity Field

At time  $t$ , the vertical axis of the rotating draft is located at  $x_c(t), y_c(t)$ , and the velocity field inside the core is given by

$$u(x, y, z, t) = U_b + \eta(t) Z + \frac{1}{2} [D(t) X(x, t) - \zeta(t) Y(y, t)] \quad (3a)$$

$$v(x, y, z, t) = V_b - \xi(t) Z + \frac{1}{2} [D(t) Y(y, t) + \zeta(t) X(x, t)] \quad (3b)$$

$$w(x, y, z, t) = w(t) = \frac{D(t)}{\epsilon} \quad (3c)$$

where  $X(x, t) = x - x_c(t)$ ,  $Y(y, t) = y - y_c(t)$ , and  $U_b$  and  $V_b$  are constants that represent the uniform part of the horizontal flow at the base of the core. The terms  $\eta(t) Z$  and  $-\xi(t) Z$  describe the vertical wind shear that corresponds to the horizontal vorticity. The terms  $-\zeta(t) Y/2$  and  $\zeta(t) X/2$  represent the inner flow of the Rankine vortex, which rotates as a solid body with angular velocity given by

$$\dot{\theta} = \frac{\zeta}{2} \quad (4)$$

The terms  $D(t) X/2$  and  $D(t) Y/2$  represent the axisymmetric horizontal radial flow that results from the divergence.

The density (eqs. (1)) and velocity (eqs. (3)) are referred to level  $b$  at the base of the core. Actually, we could use any reference level  $m$ , where  $(b \leq m \leq h)$ , by making the substitution  $(U_b, V_b, \rho_b^o, z - b) \rightarrow (U_m, V_m, \rho_m^o, z - m)$ . The velocity field (eqs. (3)) represents the zeroth- and first-order terms of a Taylor series in  $X, Y, Z$  with coefficients that are unknown functions of  $t$ . Similar solutions may exist for higher order terms of this series, which would represent more complex inner structures.

#### 3.2. Momentum Equation

The inviscid momentum equation is given by (refs. 18 and 15)

$$\frac{\partial \mathbf{v}}{\partial t} + \boldsymbol{\omega} \times \mathbf{v} + \nabla \frac{v^2}{2} = -\frac{\nabla p}{\rho} - \nabla \Phi - 2\boldsymbol{\Omega} \times \mathbf{v} \quad (5)$$

where

$\mathbf{v}$  fluid velocity,  $\text{m}\cdot\text{s}^{-1}$

$\boldsymbol{\omega}$  vorticity,  $\text{curl } \mathbf{v}$ ,  $\text{s}^{-1}$

$v^2 = \mathbf{v} \cdot \mathbf{v}$

$p$  pressure, Pa

$\rho$  density,  $\text{kg}\cdot\text{m}^{-3}$

$\Phi$  geopotential,  $gz$ ,  $\text{m}^2\cdot\text{s}^{-2}$

$g$  gravitational acceleration,  $9.81 \text{ m}\cdot\text{s}^{-2}$

$\boldsymbol{\Omega}$  angular velocity of the Earth,  $\text{rad}\cdot\text{s}^{-1}$

The left-hand side of equation (5) represents the acceleration of a fluid parcel, and the right-hand side represents the corresponding force per unit mass.

Solving equation (5) for  $\nabla p$  and substituting the inner velocity field (eqs. (3)) give

$$\begin{aligned} \frac{\partial p}{\partial x} = & -\frac{\rho}{2} \left[ \dot{D}X - \dot{\zeta}Y - D\dot{x}_c + \zeta\dot{y}_c + 2\dot{\eta}Z + 2w(\eta + 2\Omega_y) \right] \\ & + \frac{\rho}{2} (\zeta + 4\Omega_z) \left[ V_b - \xi Z + \frac{1}{2} (DY + \zeta X) \right] \\ & - \frac{\rho D}{2} \left[ U_b + \eta Z + \frac{1}{2} (DX - \zeta Y) \right] \end{aligned} \quad (6a)$$

$$\begin{aligned} \frac{\partial p}{\partial y} = & -\frac{\rho}{2} \left( \dot{D}Y + \dot{\zeta}X - \zeta\dot{x}_c - D\dot{y}_c - 2\dot{\xi}Z - 2w\xi \right) \\ & - \frac{\rho}{2} (\zeta + 4\Omega_z) \left[ U_b + \eta Z + \frac{1}{2} (DX - \zeta Y) \right] \\ & - \frac{\rho D}{2} \left[ V_b - \xi Z + \frac{1}{2} (DY + \zeta X) \right] \end{aligned} \quad (6b)$$

$$\frac{\partial p}{\partial z} = -\rho(g + \dot{w}) + 2\rho\Omega_y \left[ U_b + \eta Z + \frac{1}{2} (DX - \zeta Y) \right] \quad (6c)$$

where

$\Omega$  magnitude of angular velocity of Earth,  $\text{rad}\cdot\text{s}^{-1}$

$\Omega_y = \Omega \cos \phi$ ,  $\text{s}^{-1}$

$\Omega_z = \Omega \sin \phi$ ,  $\text{s}^{-1}$

$\phi$  latitude of local tangential frame origin, rad

and dots denote time derivatives and  $\rho$  is given by equation (1b).

### 3.3. Second-Order Partial Derivatives

Pressure jumps have been observed at gust fronts in the surface layer ( $0 < z < b$ ). (See refs. 13 and 15.) However, in the middle layer ( $b < z < h$ ), we assume that the pressure  $p$  and its first- and second-order partial derivatives are continuous functions of  $x, y, z$  (except at radius  $a$ , where  $p$  must be continuous, but its derivatives may be discontinuous). It follows that (ref. 19)

$$\left. \begin{aligned} \frac{\partial^2 p}{\partial x \partial y} &= \frac{\partial^2 p}{\partial y \partial x} \\ \frac{\partial^2 p}{\partial x \partial z} &= \frac{\partial^2 p}{\partial z \partial x} \\ \frac{\partial^2 p}{\partial y \partial z} &= \frac{\partial^2 p}{\partial z \partial y} \end{aligned} \right\} \quad (r < a, b < z < h) \quad (7)$$

### 3.4. Nonlinear Harmonic Equations

Substituting the cross derivatives of equations (6) into equations (7) with  $\Omega_y$  and  $\Omega_z$  taken to be constants, dividing by  $\rho$ , and setting the coefficients of  $X$ ,  $Y$ , and  $Z$  individually to zero in each equation give the following set of coupled, nonlinear, ordinary differential equations:

$$D(U_b - \dot{x}_c) - \zeta(V_b - \dot{y}_c) + \frac{2D}{\epsilon}\eta = -\frac{2}{\epsilon}\Omega_y D + 4\Omega_z V_b \quad (8a)$$

$$D(V_b - \dot{y}_c) + \zeta(U_b - \dot{x}_c) - \frac{2D}{\epsilon}\xi = -\frac{2}{\epsilon}\Omega_y \zeta - 4\Omega_z U_b \quad (8b)$$

$$\dot{\xi} = \frac{1}{2}[\eta(\zeta + 4\Omega_z) - D\xi] \quad (8c)$$

$$\dot{\eta} = -\frac{1}{2}[\xi(\zeta + 4\Omega_z) + D\eta] \quad (8d)$$

$$\dot{\zeta} = -D(\zeta + 2\Omega_z) \quad (8e)$$

$$\dot{D} = \frac{1}{2}[\zeta(\zeta + 4\Omega_z) - D^2] \quad (8f)$$

Equations (8c)–(8f) are equivalent to the vorticity and divergence tendency equations obtained by taking the curl and divergence of the momentum equation (5). Equations (8a) and (8b) are interpreted physically in appendix B. They can be solved for the translational velocity  $\dot{x}_c, \dot{y}_c$  of the rotating draft

$$\dot{x}_c = U_b + \frac{2}{\epsilon}\Omega_y + \frac{2}{\zeta^2 + D^2} \left[ \zeta \left( -\frac{D}{\epsilon}\xi + 2\Omega_z U_b \right) + D \left( \frac{D}{\epsilon}\eta - 2\Omega_z V_b \right) \right] \quad (9a)$$

$$\dot{y}_c = V_b + \frac{2}{\zeta^2 + D^2} \left[ \zeta \left( -\frac{D}{\epsilon}\eta + 2\Omega_z V_b \right) + D \left( -\frac{D}{\epsilon}\xi + 2\Omega_z U_b \right) \right] \quad (9b)$$

The inverse scale height  $\epsilon$  appears irreducibly in the denominator of the second term on the right-hand side of equation (9a). Therefore, this term, which results from the Coriolis force, is proportional to the scale height of the atmosphere. For the Earth, at the equator where  $\Omega_y$  is maximal, this term is about  $1 \text{ m-s}^{-1}$ . No similar term occurs in equation (9b) because  $\Omega_x = 0$ . Equations (8c)–(8f) and (9) can be integrated numerically to obtain the life cycle of the rotating draft, as is done in section 4.

### 3.5. Pressure Field

The inner pressure field  $p$  is obtained by first substituting equations (8) and (1b) into the pressure gradient (eqs. (6)) to yield

$$\frac{\partial p}{\partial x} = -\frac{\rho_b^0}{\epsilon} e^{-\epsilon Z} (1 - B) \Omega_y D \quad (10a)$$

$$\frac{\partial p}{\partial y} = \frac{\rho_b^0}{\epsilon} e^{-\epsilon Z} (1 - B) \Omega_y \zeta \quad (10b)$$

$$\frac{\partial p}{\partial z} = -\rho_b^o e^{-\epsilon Z} (1 - B) \left\{ g + \dot{w} - 2\Omega_y \left[ U_b + \eta Z + \frac{1}{2} (DX - \zeta Y) \right] \right\} \quad (10c)$$

These partial derivatives can now be integrated to obtain the inner pressure field  $p$  as

$$p(x, y, z, t) = \frac{\rho_b^o}{\epsilon} e^{-\epsilon Z} (1 - B) \left\{ g + \dot{w} - 2\Omega_y \left[ \frac{\eta}{\epsilon} + U_b + \eta Z + \frac{1}{2} (DX - \zeta Y) \right] \right\} \quad (11a)$$

The unknown buoyancy  $B(t)$  in this formula could, in principle, be determined by solving for the outer flow and equating the inner and outer pressures at the interface. As mentioned earlier, this procedure is carried through only for the basic rotating draft in appendix A. However, if we assume that the result in equation (A11) also holds here (for a rotating draft that translates), we may write

$$p(x, y, z, t) = \frac{\rho_b^o}{\epsilon} e^{-\epsilon Z} \left\{ g - 2\Omega_y \left( 1 - \frac{\dot{w}}{g} \right) \left[ \frac{\eta}{\epsilon} + U_b + \eta Z + \frac{1}{2} (DX - \zeta Y) \right] \right\} \quad (11b)$$

where  $B^2$  has been neglected. This result shows that the rotating draft has no pressure drop at its center. We shall see that the slight horizontal pressure gradient resulting from the  $\Omega_y$  term does not impede the inertial oscillation. If  $\Omega_y$  is neglected, the horizontal pressure gradient becomes zero, in agreement with the inertial oscillations treated in references 1 and 15, where  $\Omega_y$  is also neglected.

The smallness of the horizontal pressure gradient is in reasonable agreement with data from supercells without tornadoes, where the maximum horizontal pressure variation is typically about 5 mb (ref. 13). The inverse scale height  $\epsilon$  appears in the denominator of equation (11b). Therefore, as expected, the pressure at the base of the core ( $z = b$ ) is roughly proportional to the scale height of the atmosphere.

### 3.6. Thermodynamic Energy Equation

Since the density and pressure are now known, the temperature  $T$  can be determined approximately from the equation of state for a dry perfect gas

$$p = \rho RT \quad (12)$$

where  $R$ , the gas constant, equals  $287 \text{ J}\cdot\text{kg}^{-1}\cdot\text{K}^{-1}$ . The temperature is determined for the basic rotating draft in section A4.

The thermodynamic energy equation is given by (ref. 1)

$$\dot{q} = \rho c_p \left( \frac{\partial}{\partial t} + \mathbf{v} \cdot \nabla \right) T - \left( \frac{\partial}{\partial t} + \mathbf{v} \cdot \nabla \right) p \quad (13a)$$

where  $c_p$ , the specific heat at constant pressure, equals  $1004 \text{ J}\cdot\text{kg}^{-1}\cdot\text{K}^{-1}$  and  $\dot{q}$  (the diabatic heating rate in  $\text{W}\cdot\text{m}^{-3}$ ) is the heating rate per unit volume due to radiation, heat conduction, viscous dissipation, and latent heat release. For a rotating draft in the middle troposphere, the main source of diabatic heating is latent heat release and the other sources are neglected, as mentioned earlier. Since all the quantities on the right-hand side of equation (13a) are known, this equation can be used to determine the latent heat release required by the flow. The corresponding condensation rate of water vapor density  $\dot{\rho}_v$  (in  $\text{g}\cdot\text{s}^{-1}\cdot\text{m}^{-3}$ ) is given by

$$\dot{\rho}_v = \frac{\dot{q}}{L_c} \quad (13b)$$

where  $L_c$ , the latent heat of condensation, equals  $2.5 \times 10^3 \text{ J-g}^{-1}$ . The total heating and water vapor influx can be obtained by integrating equations (13a) and (13b) over the core volume, as is done for the basic rotating draft in section A4.

## 4. Numerical Integration and Supercell Solution

### 4.1. Inertial Oscillation of $\zeta$ and $D$

Equations (8e) and (8f) are coupled nonlinear equations that can be numerically integrated for  $\zeta(t)$  and  $D(t)$ . (The draft velocity  $w(t)$  is also obtained from the proportionality in eq. (2b).) When this integration is done, the solution is found to oscillate, as shown in figures 3(a) and (b). This oscillation results from the interaction of the Coriolis force with  $\zeta$  and  $D$ . Dimensional analysis shows that the period  $\tau$  (in s) is inversely proportional to  $\Omega_z$ , and the numerical solutions provide the constant of proportionality

$$\tau = \frac{\pi}{\Omega_z} \quad (14)$$

This period, which is half that of a Foucault pendulum, is characteristic of inertial oscillations (refs. 1 and 15). (In the southern hemisphere where  $\Omega_z$  is negative, the divergence  $D$ , as plotted in fig. 3(b), remains the same, but  $\zeta$ , as plotted in fig. 3(a), undergoes a sign reversal.)

The inertial oscillation described by equations (8e) and (8f) is an autonomous relaxation oscillation, as discussed in reference 20. That is, it is an unforced, nonlinear oscillation whose period consists of a long quiescent phase and a short intense phase. (For the solution shown in fig. 3(a), the intense phase is defined by  $\zeta > 0$  and the quiescent phase by  $\zeta < 0$ .) The physics of this oscillation is discussed in section 5.

The parameters and the initial values used in the numerical integration are listed in table I and were chosen to apply to a well-documented supercell storm (refs. 21 through 24). This storm, which was classified as a supercell of moderate intensity, generated hail up to 1.5 cm in diameter. The storm occurred at latitude  $41^\circ \text{ N}$ ; hence,  $\Omega_z$  equals  $4.77 \times 10^{-5} \text{ s}^{-1}$  and  $\tau = 18.3 \text{ hr}$ . The integration was started midway through the intense phase of the cycle; hence  $D(0)$  equals 0. The observed lifetime of the storm was about 5 hr. This lifetime corresponds in the model to the duration of the intense phase, which we took to be 5.33 hr. As shown in appendix C, this duration is roughly proportional to  $\zeta(0)^{-1/2}$ , and it was simulated by taking  $\zeta(0) = 3 \times 10^{-4} \text{ s}^{-1}$ . The resulting peak values for  $D(t)$  were  $\pm 1.86 \times 10^{-4} \text{ s}^{-1}$  and for  $w(t)$  were  $\pm 1.49 \text{ m-s}^{-1}$ , where we have taken  $\epsilon = 1.25 \times 10^{-4} \text{ m}^{-1}$ . These values are reasonable for spatial averages in the core of the supercell, as is explained in section 4.3.

When equations (8e) and (8f) are written in the conservative form,

$$\frac{\partial A}{\partial t} + \text{div} A \mathbf{v} = S_A \quad (15a)$$

where  $A$  represents  $\zeta$  or  $D$  (or any other scalar or vector component), the supply terms for  $\zeta$  and  $D$  are found to be

$$S_\zeta = -2D\Omega_z \quad (15b)$$

$$S_D = \frac{1}{2} (D^2 + \zeta^2) + 2\Omega_z \zeta \quad (15c)$$

Therefore, the interaction of  $D$  with  $\Omega_z$  supplies the vertical component of vorticity  $\zeta$ . This supply is positive when  $D$  and  $w$  are negative; that is, during the downdraft phase, in agreement with figures 3(a) and (b). The supply of corresponding angular momentum density  $L_z = (\mathbf{r} \times \rho \mathbf{v}) \cdot \hat{\mathbf{z}}$  in the core is found by substituting  $L_z$  for  $A$  in equation (15a) and is

$$S_{L_z} = -2\Omega_z r \rho v_r \quad (15d)$$

where  $v_r$ , the radial flow resulting from  $D$ , is  $Dr/2$ . Therefore, the action of  $\Omega_z$  on the horizontal radial flow supplies the angular momentum. Again, this supply is positive when  $v_r$ ,  $D$ , and  $w$  are all negative.

The implication of figures 3(a) and (b) for an actual supercell is that its rotation rate increases when the vertical flow in the middle troposphere is predominantly downward and decreases when this flow becomes predominantly upward. In the model, the transition from downdraft to updraft occurs in the middle of the intense phase when  $w(t) = 0$ , as shown in figure 3(b). For a supercell, this “transition point” is envisioned to occur when the decaying downdraft and the growing updraft form a couplet whose spatial average is momentarily zero.

By equation (15c), the interaction of  $\zeta$  (or the corresponding azimuthal flow) with  $\Omega_z$  contributes to the supply of  $D$ . This contribution causes  $D$  to become positive in the middle of the intense phase and negative in the middle of the quiescent phase, as also shown in figure 3(b), so that the cycle repeats.

#### 4.2. Buoyancy

The supply of kinetic energy density  $\text{KE} = \frac{1}{2}\rho\mathbf{v} \cdot \mathbf{v}$  in the core of the rotating draft is given by (eq. (15a))

$$S_{\text{KE}} = -\mathbf{v} \cdot \nabla p - \rho w g \quad (16a)$$

Substituting the pressure given by equation (11b), with the  $\Omega_y$  term and  $B^2$  neglected, gives

$$S_{\text{KE}} = w f_B \quad (16b)$$

where  $f_B$  is the buoyant force density given by equation (1d). Therefore, the buoyant force acting on the draft supplies the kinetic energy for the fluid in the core. The net supply of kinetic energy over one complete cycle is zero.

For the basic rotating draft that does not translate, the buoyancy is given by equation (A11) as  $B = \dot{w}/g$ . If we assume that this expression also holds during translation, we may compute  $B$  by referring to equations (2b) and (8f) as

$$B = \frac{1}{2\epsilon g} \left[ \zeta (\zeta + 4\Omega_z) - D^2 \right] \quad (17)$$

A plot of  $B$  against  $t$  for the supercell solution is shown in figure 3(c). Comparison of figures 3(c) and (b) shows that the downdraft which initiates the intense phase results from a weakly negative buoyant force acting for a long time and that the transition to an updraft results from a stronger positive buoyant force acting for a short time. The peak positive buoyancy corresponds to an average temperature excess in the core of 0.016 K, as also shown in figure 3(c).

#### 4.3. Core Radius $a$ and Angular Displacement $\theta$

Again we assume that a result that holds for the basic rotating draft can also be applied to the translating solution. With  $\zeta(t)$ ,  $D(t)$ , and  $w(t)$  known, equations (A3) and (4) can be numerically integrated to obtain the core radius  $a(t)$  and the angular displacement of the core fluid  $\theta(t)$  from the initial values  $a(0) = 13.8$  km and  $\theta(0) = 0$  rad, as shown in figures 3(d) and (e). This value for  $a(0)$  gives the measured mass inflow rate of  $\dot{M} = 1.30 \times 10^9$  kg-s<sup>-1</sup> for  $w = 1.49$  m-s<sup>-1</sup> (its maximum value). This updraft maximum occurs at  $t = 5$  ks, when the core radius  $a = 19.0$  km, which agrees well with the observed radius of 20 km. (See ref. 21.) For this calculation, we used reported values for the height of the core base  $b = 4.43$  km above mean sea level, for the density at this height  $\rho_b^0 = 0.77$  kg/m<sup>3</sup>, and for the corresponding pressure  $p(b) = 6.05 \times 10^4$  Pa. The value  $\epsilon = 1.25 \times 10^{-4}$  m<sup>-1</sup> was then determined by using

the dominant (first) term of the pressure formula (11b). The value chosen for  $a(0)$  also gives the rotating draft a maximum circulation at  $t = 0$  of  $\Gamma(0) = \pi a(0)^2 \zeta(0) = 1.80 \times 10^5 \text{ m}^2\text{-s}^{-1}$ , which agrees reasonably well with typical measured values for supercells. (See ref. 13.)

Comparing figures 3(a) and (d) shows that the radius  $a(t)$  contracts to its minimum value as  $\zeta(t)$  reaches its peak value and expands as  $\zeta(t)$  decreases; this is in agreement with supercell observations in reference 13. According to the model, this contraction and spin-up occur during the downdraft phase, as shown in figure 3(b). The contraction is caused by the horizontal convergence that results from the compression of sinking air parcels. The horizontal convergence also interacts with the Coriolis force to produce the cyclonic spin-up. The model suggests that a predominantly downward flow causes the contraction and spin-up of a supercell storm. However, the data are inconclusive about this predominantly downward flow, as discussed in section 4.7.

#### 4.4. Diabatic Heating and Moisture Influx

In order to carry out the diabatic heating and water vapor calculations for the supercell solution (again assumed to be the same as for the basic solution) in section A4, we need to know the height  $h$  of the upper layer, as shown in figure 2. Although the visible cloud reached a height of 12.4 km (ref. 21), the height of the upper layer was estimated as  $h = 8$  km from range-height indication (RHI) radar echo profiles given in the reference. Also given are the temperatures  $T = 253$  K at height  $h$  and  $T = 273$  K at height  $b$ .

The diabatic heating is given by equation (A21), where  $\dot{Q}(t)$  (in W) is the total heat per second supplied to the core. This result for  $\dot{Q}$  is plotted against  $t$  in figure 3(f). Also shown in this figure is the corresponding water vapor influx  $\dot{M}_v$  (in  $\text{g-s}^{-1}$ ), as given by equation (A22). The net supply of diabatic heating or water vapor over one complete cycle is zero. (Figs. 3(a)–(f) show that  $\zeta(t)$ ,  $B(t)$ , and  $a(t)$  are symmetric functions about the points  $t = n\tau/2$ , where  $n = 0, 1, 2, \dots$  and  $D(t)$ ,  $w(t)$ ,  $\theta(t)$ ,  $\dot{Q}(t)$ , and  $\dot{M}_v(t)$  are antisymmetric.)

The solid circles in figure 3(f) mark the points where  $w = 1.49 \text{ m-s}^{-1}$  (its maximum value). The corresponding value  $\dot{M}_v = 6.28 \times 10^9 \text{ g-s}^{-1}$  agrees reasonably well with the measured net water vapor influx of  $8.5 \times 10^9 \text{ g-s}^{-1}$  (ref. 21). Although  $w$  subsequently decreases (as shown in fig. 3(b)), figure 3(f) shows that  $\dot{M}_v$  continues to increase, and it reaches its peak value during the quiescent phase. This feature of figure 3(f) is discussed further in section 4.7.

#### 4.5. Constant of the Motion and Froude Number

The scalar resultant of the vortex and divergent flows has its maximum value at radius  $a$ . This flow speed, denoted  $v^a(\zeta, D)$ , is a constant of the motion and is given by

$$v^a(\zeta, D) = \frac{a}{2} (\zeta^2 + D^2)^{1/2} \quad (18a)$$

Its constancy is easily verified by differentiating with respect to  $t$  and substituting the tendency equations (8e), (8f), and (A3). The constancy of  $v^a(\zeta, D)$  is consistent with inertial flow as described in section 5.

For the supercell solution,  $v^a(\zeta, D)$  equals  $2.07 \text{ m-s}^{-1}$ . Because this value is a constant of the motion, the axisymmetric part of the horizontal flow in the middle layer ( $b < z < h$ ) is not intensified as the core radius  $a(t)$  contracts. The draft, however, is intensified, as shown in figure 3(b). Because the streamlines of the draft extend into the surface layer ( $0 < z < b$ ), the horizontal flow in the surface layer is also intensified as the core contracts.

From the constant of the motion given by equation (18a), the inverse scale height  $\epsilon$ , and the gravitational acceleration  $g$ , we can define a Froude number  $F$  by

$$F = \frac{\epsilon a^2}{4g} (\zeta^2 + D^2) \quad (18b)$$

where  $F$  is also a constant of the motion. This Froude number is used in the outer solution of appendix A. For the supercell solution,  $F$  equals  $5.48 \times 10^{-5}$ .

#### 4.6. Horizontal Vorticity Components $\xi$ and $\eta$

The horizontal vorticity tendency equations (8c) and (8d) can be integrated numerically to obtain  $\xi(t)$  and  $\eta(t)$  in the core of the rotating draft. These equations show that if  $\xi$  and  $\eta$  are initially zero, they will remain zero. However, if not zero, they too will oscillate, being forced by the inertial oscillation of  $\zeta$  and  $D$ , as shown in figures 3(g), (h), and (i). The horizontal vorticity vector rotates anticyclonically with changing amplitude and rotation rate. (It rotates cyclonically for an anticyclonic rotating draft, as discussed in section C2.) Its rotation rate is rapid during the intense phase and slow during the quiescent phase.

Our choice of initial values,  $\xi(0) = -1.74 \times 10^{-4} \text{ s}^{-1}$  and  $\eta(0) = 9.85 \times 10^{-4} \text{ s}^{-1}$ , will be explained later. Figure 3(i) shows that the computed inner horizontal vorticity has a maximum value of about  $1 \times 10^{-3} \text{ s}^{-1}$ , which is about one fifth the measured horizontal vorticity in the environmental flow of the supercell. (See ref. 21.)

The supplies of  $\xi$  and  $\eta$  are given by

$$S_\xi = \frac{1}{2} [D\xi + \eta(\zeta + 4\Omega_z)] \quad (19a)$$

$$S_\eta = \frac{1}{2} [D\eta - \xi(\zeta + 4\Omega_z)] \quad (19b)$$

The first term on the right-hand side of both equations represents stretching of horizontal vorticity, and the second term represents tilting of vertical vorticity.

#### 4.7. Translation $\dot{x}_c, \dot{y}_c$ and Track $x_c, y_c$

At this point, all the quantities in the translation equations (9) are known, and  $\dot{x}_c(t), \dot{y}_c(t)$  can be plotted, as shown in figures 3(j), (k), and (l). These equations also can be integrated to obtain  $x_c(t), y_c(t)$ , which describe the track of the rotating draft, as shown in figures 3(m), (n), and (o). The eastward drift of the looping track shown in figure 3(o) results from the constant term  $2\Omega_y/\epsilon$  in equation (9a), which for this computation has the value  $0.88 \text{ m-s}^{-1}$ . The contributions of  $U_b, V_b$  to the drift integrate to zero during each cycle, although these constants do affect the translation during phases of the cycle, including the intense phase. The values  $U_b = 8.33 \text{ m-s}^{-1}$  and  $V_b = 1.42 \text{ m-s}^{-1}$  were chosen to simulate the mean translation observed for the supercell—about  $14 \text{ m-s}^{-1}$  from the west-southwest.

Figure 4(a) shows an aerial sequence of core images superimposed to scale for 1 cycle of the supercell solution. Figure 4(b) shows the corresponding side views with the vertical dimension exaggerated and the relative environmental flow not shown. The computational time  $t$  (fig. 3) is correlated with mountain daylight time in table II for comparison with the radar data shown in figure 5.

The sudden change in  $\dot{x}_c(t), \dot{y}_c(t)$  midway through the intense phase causes the right turn in the track, which is a salient feature of supercells. Klemp (ref. 12) states “The mechanism that causes the transverse propagation of supercell storms has remained an intriguing although illusive issue over the years.” The inertial oscillation offers the following insight.

The turning point for each cycle in figure 3(o) is defined as the midpoint of the right-turning arc. Comparing figures 3(k) and (b) shows that this turning point is the same as the transition point for the draft. The coincidence of these two points is confirmed by equation (9b). The change in  $\dot{y}_c(t)$  results from the draft velocity  $w(t) = \frac{D(t)}{\epsilon}$  interacting with the horizontal vorticity  $\xi(t), \eta(t)$ . The right turn occurs as  $D$  and  $\xi$  change signs and  $\zeta$  and  $\eta$  remain positive; that is, the right turn results from a rapid reversal of the downdraft interacting with a rapid anticyclonic rotation (through about a quarter turn) of the inner horizontal vorticity vector. Other treatments of supercells have also linked their transverse propagation to the horizontal vorticity or vertical wind shear (refs. 2 and 11).

For an anticyclonic rotating draft with otherwise identical initial conditions (section C2), the plots for  $D$  and  $\eta$  would be about the same as those shown in figures 3(b) and (h). However, the plots of  $\zeta$  and  $\xi$  are approximately mirror images of figures 3(a) and (g). Consequently, the track turns to the left, which is also in agreement with observation (ref. 3); that is, the left turn of an anticyclonic rotating draft results from a rapid reversal of the downdraft interacting with a rapid cyclonic rotation of the inner horizontal vorticity vector.

The initial values  $\xi(0), \eta(0)$  were chosen to simulate the  $33^\circ$  rightward turn of the documented supercell. Figure 5 shows the computed track (one cycle from fig. 3(o)) superimposed on radar echoes of the supercell obtained at 30-min intervals. The turning point occurred at 1602 MDT when the supercell crossed the Wyoming-Nebraska boundary. According to the theory, this turning point is the same as the transition point for the draft; that is, west of the Wyoming-Nebraska boundary the computed draft (fig. 3(b)) is downward (which corresponds to an actual vertical flow that is predominantly downward) and to the east it is upward.

Data support the solution east of the turning point. A net upward mass flux of  $1.30 \times 10^9 \text{ kg-s}^{-1}$  (as mentioned in section 4.3) was measured during the period from 1614 to 1700 MDT by two circumnavigating aircraft in the surface layer. (See ref. 21.)

However, no similar measurements were made west of the turning point to detect the predominantly downward flow indicated by the solution. The corresponding radar echoes depict only the condensed moisture in the nascent, rapidly growing updraft. The downdraft that (according to the theory) dominated the vertical flow at this time and caused the developing supercell to contract and spin up would probably have been invisible to radar. Therefore, the reported data are inconclusive about this predominantly downward flow west of the turning point, which is an important feature of the solution.

The data also do not appear to support the solution during the quiescent phase before 1323 MDT and after 1841 MDT. Two possible explanations are offered for this apparent discrepancy:

1. As mentioned in section 4.4, the theoretical water vapor influx shown in figure 3(f) continues to increase until 2036 MDT, which is almost 2 hr after the onset of the quiescent phase. Suppose that the actual supply of water vapor to the supercell should fall short after 1841 MDT. After that time, the mathematical solution would no longer be physically valid. A similar explanation applies before 1323 MDT. The quiescent phase of the solution was not observed, possibly because the quiescent phase required more latent energy than was available.
2. As mentioned in section 2.2, we have assumed that the inner solution for a rotating draft that translates can always be matched to the environmental flow. During the intense phase, the relative environmental flow can be blocked by the flow in the core so that the matching assumption is satisfied; however, at the onset of the quiescent phase, as the track turns northward and westward (into the environmental flow), the blocking fails, matching becomes impossible, and the core is blown away. A similar explanation applies

before 1323 MDT. The quiescent phase of the solution was not observed, possibly because during the quiescent phase the inner solution could not be matched to the environmental flow.

Therefore, only the intense phase of the inertial oscillation appears to be relevant to a supercell. Essentially all the adjustable parameters in the model ( $\xi(0)$ ,  $\eta(0)$ ,  $\zeta(0)$ ,  $a(0)$ ,  $U_b$ , and  $V_b$ ) were required to simulate the duration, diameter, vortex circulation, vertical mass flux, water vapor influx, translational velocity, and track of the documented supercell.

## 5. Physics of Inertial Oscillation

### 5.1. Inertial Flow

We restrict the discussion in this section to the basic rotating draft, whose inertial oscillation is described mathematically by equations (4), (8e), (8f), (A3), (A11), and (A20) for  $\theta(t)$ ,  $\zeta(t)$ ,  $D(t)$ ,  $a(t)$ ,  $B(t)$ , and  $\dot{Q}(t)$ , with  $U_b = V_b = \Omega_y = \xi = \eta = 0$ . One solution of these equations is given in section 4, and several more are described in appendix C. Now we address the physics of these solutions, as shown in figure 6.

A Rankine vortex in an inertial frame has a pressure drop at the center; however, the result (eq. (A13)) for the basic rotating draft in a local tangential frame of the Earth (fig. 1) shows that the horizontal pressure gradient in the core is zero—a characteristic of inertial flow. As described in references 1 and 15, inertial flow is frictionless horizontal flow wherein a fluid parcel moves with constant speed  $v_i$  along a circular arc such that the centrifugal force balances the Coriolis force. The inertial radius  $R_i$  of the circular arc is then given (in m) by

$$R_i = \frac{v_i}{2\Omega_z} \quad (20)$$

where  $\Omega_z$  in general varies with latitude. If  $R_i$  is sufficiently small (as in a supercell), the variation in  $\Omega_z$  may be neglected, and the parcel traverses a circle, as shown in figure 6(a). The motion is anticyclonic, and the period is given by  $\pi/\Omega_z$ , which is the same as the period of the rotating draft (eq. (14)). In the following examples, we take  $\Omega_z = 4.77 \times 10^{-5} \text{ s}^{-1}$ , as in the supercell solution.

### 5.2. Contraction and Cyclonic Spin-Up

Figure 6(b) shows an aerial view of the core of the rotating draft at its maximum radius  $a_2 = 57.3 \text{ km}$ . At this time,  $D_2 = 0$ ,  $\zeta_2 = -7.24 \times 10^{-5} \text{ s}^{-1}$ , and the flow is momentarily that of an anticyclonic Rankine vortex with no radial nor vertical flow. The speed  $v_i$  of a parcel on the periphery of the core is given (in  $\text{m}\cdot\text{s}^{-1}$ ) by

$$v_i = \frac{|\zeta_2|a_2}{2} = 2.07 \quad (21)$$

and its inertial radius is given by

$$R_i = \frac{|\zeta_2|a_2}{4\Omega_z} = 2.17 \times 10^4 \quad (22)$$

The inward track (projected on a horizontal plane) of parcels on the periphery of the core is shown in figure 6(c). The inertial motion causes the core to contract and spin up cyclonically. Maximum contraction and spin-up are achieved when the parcels have traversed a semicircle. According to this physical picture, the minimum core radius  $a_1$  is given by

$$a_1 = a_2 - 2R_i = 1.38 \times 10^4 \quad (23)$$

which agrees with the value obtained in section 4 by integrating the differential equations. Since the inertial speed  $v_i$  of a parcel is constant, the maximum vorticity  $\zeta$  (in  $\text{s}^{-1}$ ) and Rossby number  $\text{Ro}_1$  are given by

$$|\zeta_1| = |\zeta_2| \frac{a_2}{a_1} = 3.0 \times 10^{-4} \quad (24a)$$

$$\text{Ro}_1 = \frac{|\zeta_1|}{2\Omega_z} = 3.14 \quad (24b)$$

which also agree with the values computed in section 4.

During the contraction and spin-up, each parcel in the core is compressed by descending in the spatially uniform downdraft. When the core radius reaches its minimum value, the compression ceases, and the downdraft also ceases before reversing. These physical observations are in agreement with the draft velocity  $w(t)$  shown in figure 3(b).

A complete cycle of the inertial oscillation is depicted physically in figure 6(d). (This figure corresponds to the computations shown in figs. 3(a)–(e).) The total angular excursion of the core fluid during 1 cycle can be determined by drawing both tangents to an inertial circle from the center of the rotating draft, as shown. The included angle  $\alpha$  is 1.32 rad, in agreement with the numerical integration shown in figure 3(e).

The duration of the intense phase ( $\zeta > 0$ ) can be determined from the angle  $\beta$  in figure 6(d). Since  $\beta = 1.82$  rad and the period  $\tau = 18.3$  hr, the duration of the intense phase is 5.33 hr, in agreement with the numerical integration shown in figure 3(a).

### 5.3. Increased Contraction and Cyclonic Spin-Up

If we hold  $a_2$  and  $\Omega_z$  fixed but increase the magnitude of the initial anticyclonic vorticity by taking  $\zeta_2 = -9.25 \times 10^5 \text{ s}^{-1}$ , the inertial radius increases to  $R_i = 26.3$  km, as depicted in figure 6(e). The contraction and cyclonic spin-up are now much greater, and the maximum Rossby number, as determined from equation (24b), is  $\text{Ro}_1 = 31.4$ , in agreement with figure 7. The peak draft speed is now  $12 \text{ m-s}^{-1}$  and the buoyancy corresponds to a maximum temperature excess of 1.06 K, as shown in figures 7(b) and (c).

The angular excursion of the core fluid, as determined from angle  $\alpha$ , has increased to 2.44 rad, in agreement with figure 7(e). The duration of the intense phase, as determined from angle  $\beta = 0.69$  rad, has decreased to 2.03 hr, in agreement with figure 7(a). Figures 6(e) and 7(a)–(e) show how the Coriolis force—in concert with the buoyant force—can effect rapid spin-ups of a vertical rotating draft by means of this inertial oscillation.

### 5.4. Singular Point

If we continue to increase the inertial radius  $R_i$  by increasing  $|\zeta_2|$  (with  $a_2$  and  $\Omega_z$  held fixed), we soon approach a singular point where  $R_i = a_2/2$ , which corresponds to  $\zeta_2 = -2\Omega_z$ . This is the singularity that separates the two solution domains of equations (8e) and (8f), as discussed in section C2.

### 5.5. Anticyclonic Spin-Up

If  $R_i$  is increased past the singular point by taking  $\zeta_2 = -2.63 \times 10^{-4} \text{ s}^{-1}$ , the inertial oscillation produces anticyclonic spin-up, as shown in figure 6(f). This anticyclonic spin-up corresponds to the second solution domain of equations (8e) and (8f), as discussed in section C2 and illustrated in figure 8.

## 5.6. Steady-State Anticyclonic Rankine Vortex

If  $R_i$  is further increased to equal  $a_2$ , as shown in figure 6(g), no contraction nor spin-up occurs, and the inertial motion corresponds to a steady-state anticyclonic Rankine vortex of vorticity  $\zeta = -4\Omega_z \text{ s}^{-1}$ , as discussed in section C3.

Further increases in  $R_i$  correspond to anticyclonic spin-up, as already discussed, except that the initial radius  $a_2$  becomes the minimum radius of the oscillating core. In conclusion, the physics of inertial motion, as shown in figures 6(d)–(g), corresponds exactly to the mathematical solutions given in section 4 and appendix C.

## 6. Implications for Numerical Simulations

Current numerical supercell simulations (refs. 8 through 13) do not depend on the Coriolis force, but generate rotation by using a buoyant plume to lift and stretch local horizontal vortex lines, as suggested in reference 25. This mechanism produces two counterrotating cells that split, after which one cell often intensifies and the other decays. However, Klemp and Wilhelmson (ref. 9) state “It should be emphasized that although we have simulated self-sustaining single-cell storms, there is no evidence that other single-cell structures cannot exist which produce similar storm longevity. In particular, the storms simulated here evolve through a splitting process. For storms which do not split, other opportunities may arise for generating a self-sustaining structure.”

One of the “other opportunities” referred to could be the inertial oscillation of a vertical rotating draft described herein. Perhaps the intense phase of this oscillation could be excited in a numerical simulation that includes (1) the Coriolis force, (2) fully compressible equations, (3) abundant water vapor in the surface layer, and (4) initialization with a plume that is large in diameter and negatively buoyant. The negative buoyancy would induce a compressible downdraft that, in turn, would cause horizontal convergence in the middle tropospheric layer. The Coriolis force, acting on this convergent flow, would spin up the cell. Concurrently, the gust front from the downdraft would lift the moisture-laden surface air, causing condensational heating that would initiate an updraft. The updraft would rapidly grow and become predominant until, at the end of the intense phase, the cell dissipates. The numerical simulation could additionally include horizontal flow with vertical wind shear to make the track of the cell turn to the right.

## 7. Concluding Remarks

The most surprising result of this theoretical research is the discovery that a vertical rotating draft can undergo an inertial oscillation, whereby the Coriolis force can quickly generate high Rossby number flows (cyclonic or anticyclonic). The oscillation is nonlinear, and each period consists of a long quiescent phase when the core is large in diameter and rotates anticyclonically and a short intense phase when the core is small and rotates either cyclonically or anticyclonically. The oscillation is explained physically by horizontal inertial flow that is coupled with compressible vertical flow.

The inertial oscillation is engendered by (1) a constant Coriolis parameter, (2) air density that decreases exponentially with height, (3) inviscid, compressible flow, (4) a vertical draft, (5) vertical vorticity in the draft, (6) horizontal divergence in the draft, (7) buoyancy, and (8) diabatic heating. These ingredients are similar to the gross characteristics of a supercell storm. During the intense phase of the inertial oscillation, the vertical rotating draft has features that agree with supercell observations, which are

1. The diameter of the core contracts as its rotation rate increases and expands as it decreases
2. If vertical wind shear is included, the track of the rotating draft turns to the right (an anticyclonic rotating draft turns to the left)

3. This turning point is followed by a predominantly upward flow
4. The horizontal pressure gradient is very small (a property of most tornadoless supercells)

When the solution was applied to a documented supercell, reasonable agreement was obtained for the longevity of the storm, its diameter, vortex circulation, vertical mass flux, water vapor influx, translational velocity, and storm track. However, the data did not appear to support the quiescent phase of the oscillation, and reasons for this discrepancy are suggested. A critical experiment would measure the predominantly downward flow that theoretically occurs before the turning point in a supercell track and causes contraction and spin-up. Means are also suggested for exciting the intense phase of this inertial oscillation in numerical simulations of supercells.

NASA Langley Research Center  
Hampton, VA 23681-0001  
July 17, 1992

## Appendix A

### Basic Rotating Draft That Oscillates But Does Not Translate

#### A1. Basic Inner Solution

For the rotating draft to remain centered on the origin (i.e., for  $x_c(t) = y_c(t) = 0$ ), we must take  $U_b = V_b = \Omega_y = \xi = \eta = 0$ . The tendency equations (9), (8c), and (8d) for the inner solution of the middle layer ( $r \leq a$ ,  $b < z < h$ ) then become  $\dot{x}_c = \dot{y}_c = \dot{\xi} = \dot{\eta} = 0$ . Note that equations (8e) and (8f), which give the inertial oscillation, are unaffected.

The inner density remains as given by equation (1b); however, the pressure (eq. (11a)) and velocity field (eqs. (3)) become, in cylindrical coordinates

$$p(r, \theta, z, t) = \frac{g}{\epsilon} \rho_b^o e^{-\epsilon Z} [1 - B(t)] \left[ 1 + \frac{\dot{w}(t)}{g} \right] \quad (\text{A1a})$$

$$v_r(r, \theta, z, t) = \frac{D(t)}{2} r \quad (\text{A1b})$$

$$v_\theta(r, \theta, z, t) = \frac{\zeta(t)}{2} r \quad (\text{A1c})$$

$$v_z(r, \theta, z, t) = \frac{D(t)}{\epsilon} \quad (\text{A1d})$$

#### A2. Outer Solution

Using the Rankine vortex as a model, we take the external vorticity  $\omega^o$  and divergence  $D^o$  to be zero. Hence, the outer velocity field in the middle layer ( $a \leq r$ ,  $b < z < h$ ) is given by

$$v_r^o(r, \theta, z, t) = \frac{D(t) a^2(t)}{2r} \quad (\text{A2a})$$

$$v_\theta^o(r, \theta, z, t) = \frac{\zeta(t) a^2(t)}{2r} \quad (\text{A2b})$$

$$v_z^o(r, \theta, z, t) = 0 \quad (\text{A2c})$$

The field  $v_r$  is continuous at the interface  $r = a$ , as required by the jump conditions for the continuity and momentum equations. The field  $v_\theta$  is also continuous, but  $v_z$ ,  $\rho$ ,  $D$ , and  $\zeta$  have finite discontinuities. The requirement that the interface move with the fluid gives

$$\dot{a} = \frac{Da}{2} \quad (\text{A3})$$

which will determine the core radius  $a(t)$ . Still to be imposed is the jump condition that the pressure  $p$  be continuous at  $r = a$ , which will determine the core buoyancy  $B(t)$ .

A sequence in figure 9 depicts the inertial oscillation of the horizontal flow in a basic rotating draft. The initial conditions on  $\zeta$ ,  $D$ , and  $a$  are the same as in the supercell solution of section 4, and the sequence in figure 9 corresponds to the core sequence shown in figure 4, except that the flows at 1523 and 1641 MDT are omitted.

Solving the momentum equation (5) for the pressure gradient in cylindrical coordinates and substituting the outer velocity field from equations (A2) and the tendencies in equations (A3), (8e), and (8f) give

$$\frac{\partial p^o}{\partial r} = -\frac{gF\rho^o}{\epsilon r} \left(1 - \frac{a^2}{r^2}\right) \quad (\text{A4a})$$

$$\frac{\partial p^o}{\partial \theta} = 0 \quad (\text{A4b})$$

$$\frac{\partial p^o}{\partial z} = -g\rho^o \quad (\text{A4c})$$

where  $F$ , the Froude number, is a constant of the motion given by equation (18b).

As with the inner solution, we require

$$\frac{\partial^2 p^o}{\partial r \partial z} = \frac{\partial^2 p^o}{\partial z \partial r} \quad (a < r, b < z < h) \quad (\text{A5})$$

As a consequence, the outer density  $\rho^o$  must satisfy

$$\frac{\partial \rho^o}{\partial r} = \frac{F}{\epsilon r} \left(1 - \frac{a^2}{r^2}\right) \frac{\partial \rho^o}{\partial z} \quad (\text{A6})$$

A solution of this equation is given by

$$\rho^o = \frac{C(t)}{r^F} \exp\left(-\epsilon Z - \frac{Fa^2}{2r^2}\right) \quad (\text{A7})$$

where  $C(t)$  can be determined from the boundary value (eq. (1a)):

$$C(t) = \rho_b^o a^F e^{F/2} \quad (\text{A8})$$

Hence, the outer density is given for the middle tropospheric layer by

$$\rho^o(r, \theta, z, t) = \rho_b^o \left(\frac{a}{r}\right)^F \exp\left[-\epsilon Z + \frac{F}{2} \left(1 - \frac{a^2}{r^2}\right)\right] \quad (\text{A9a})$$

Integrating for the outer pressure gives finally

$$p^o(r, \theta, z, t) = \frac{g}{\epsilon} \rho_b^o \left(\frac{a}{r}\right)^F \exp\left[-\epsilon Z + \frac{F}{2} \left(1 - \frac{a^2}{r^2}\right)\right] \quad (\text{A9b})$$

Because of the smallness of  $F$  (section 4.5), these outer pressure and density fields are essentially independent of  $r$  far beyond the 60-km radial limit of the validity of the cylindrical frame for meteorological flows. As  $r \rightarrow \infty$ ,  $p^o$  and  $\rho^o$  remain bounded, as required. In fact, both slowly approach zero in this limit. A corollary of equations (A9a) and (A9b) is that

$$p^o = \frac{g}{\epsilon} \rho^o \quad (\text{A9c})$$

Upon substitution of equations (A2) and (A9a), the continuity equation (2a) indicates that air is being entrained into the outer part of the middle tropospheric layer from the surface and upper layers at the rate (see eq. (15a))

$$S_\rho^o = \rho^o \frac{FD}{2} \left(1 - \frac{a^2}{r^2}\right)^2 \quad (\text{A10a})$$

where  $S_\rho^o$  is in units of  $\text{kg}\cdot\text{s}^{-1}\cdot\text{m}^{-3}$ , and  $\rho^o$  is given by equation (A9a). Because  $a(t)$  is a symmetric function of  $t$  and  $D(t)$  is antisymmetric, the net entrainment over a complete cycle is zero. For the supercell solution, the maximum mass entrained during one half cycle is less than 1 percent of the mass already present in the middle layer. Hence, the mass entrainment is negligible, and any momentum exchange resulting from it is also negligible.

The radial pressure gradient and radial velocity supply kinetic energy to the outer flow at the rate (in  $\text{W}\cdot\text{m}^{-3}$ )

$$S_{\text{KE}}^o = -v_r^o \frac{\partial p^o}{\partial r} = \frac{\rho^o g F D a^2}{2\epsilon r^2} \left(1 - \frac{a^2}{r^2}\right) \quad (\text{A10b})$$

where  $\text{KE} = \frac{1}{2}\rho^o[(v_r^o)^2 + (v_\theta^o)^2]$ . Again, the net kinetic energy supplied over a cycle is zero.

The interaction of the radial velocity with  $\Omega_z$  again supplies the angular momentum about the  $z$ -axis, as given for the outer flow by

$$S_{L_z}^o = -2\Omega_z r \rho^o v_r^o = -\Omega_z \rho^o D a^2 \quad (\text{A10c})$$

where  $L_z^o = (\mathbf{r} \times \rho^o \mathbf{v}^o) \cdot \hat{z}$ . Within the limitations of the cylindrical coordinate frame, these velocity, pressure, and density fields constitute a satisfactory outer solution for the basic rotating draft that oscillates inertially at a fixed location.

### A3. Buoyancy and Inner Pressure

The buoyancy  $B(t)$  can now be determined by the requirement of pressure continuity at  $r = a$ . Equating equations (A1a) and (A9b) for  $r = a$  gives

$$B(t) = \frac{\dot{w}(t)}{g} \quad (\text{A11})$$

where we have used the assumption that  $B \ll 1$ . Equation (1d) then gives

$$f_B = \rho \dot{w} \quad (\text{A12})$$

where again  $B^2$  has been neglected. Therefore, the vertical acceleration of the core fluid is exactly balanced by the buoyant force. The corresponding inner pressure, as given by equation (A1a), is now independent of  $t$  and may be written as

$$p = \frac{g}{\epsilon} \rho_b^o e^{-\epsilon Z} \quad (\text{A13})$$

where again  $B^2$  has been neglected.

### A4. Temperature, Diabatic Heating, and Moisture Influx

Because the density and pressure are now known, we can determine the approximate temperature from the equation of state for a dry perfect gas (eq. (12)). In the outer region, this equation becomes

$$p^o = \rho^o R T^o \quad (\text{A14})$$

Substituting equation (A9c) and solving for  $T^o$  gives (in K)

$$T^o = \frac{g}{\epsilon R} = 273 \quad (\text{A15})$$

Therefore, the outer solution applies to an isothermal middle troposphere.

In the core, substitution of the density (eq. (1b)) into the equation of state (eq. (12)) gives

$$p = \rho_b^o RT (1 - B) e^{-\epsilon Z} \quad (\text{A16})$$

Eliminating  $p$  from this expression and the inner pressure (eq. (A13)) enables us to solve for the inner temperature

$$T(t) = T^o [1 + B(t)] \quad (\text{A17})$$

where  $B^2$  has been neglected and  $T^o$  is given by equation (A15). Hence, the core is also isothermal, but its temperature varies with time to give the buoyancy shown in figure 3(c).

Heat must be supplied to the fluid in the core to effect the temporal changes in  $T(t)$  and to maintain the isothermal state of rising and expanding air parcels. The supply of heat  $\dot{q}$  (in  $\text{W}\cdot\text{m}^{-3}$ ) is given by the thermodynamic energy equation (13a). If the inner pressure (eq. (A13)) and temperature (eq. (A17)) are substituted, this equation becomes

$$\dot{q} = \rho c_p T^o \dot{B} - w \frac{\partial p}{\partial z} \quad (\text{A18})$$

However, this result overestimates the heating required by a supercell because of the temperature lapse rate in the middle troposphere. The temperature in the documented supercell (ref. 21) decreased from 273 K at  $b = 4.43$  km to 253 K at  $h = 8$  km. If we assume that the vertical rotating draft solution remains valid regardless of this 7-percent departure from isothermality, we can use the original energy equation (13a) to incorporate the temperature lapse rate as shown

$$\dot{q} = \rho c_p T^o \dot{B} + \rho c_p w \frac{\partial T}{\partial z} - w \frac{\partial p}{\partial z} \quad (\text{A19})$$

where  $\partial T/\partial z = -5.6 \times 10^{-3} \text{ K}\cdot\text{m}^{-1}$ . (The correction to  $\dot{q}$  is about 50 percent, whereas the error introduced by neglecting the lapse rate in the first and third terms on the right-hand side of equation (A19) is small (about 4 percent after the integration to follow).)

Integrating equation (A19) over the volume of the core gives the total diabatic heating rate  $\dot{Q}(t)$  (in W) as

$$\begin{aligned} \dot{Q} &= \pi a^2 c_p \left( T^o \dot{B} + w \frac{\partial T}{\partial z} \right) \int_b^h \rho dz - \pi a^2 w [p(h) - p(b)] \\ &= \left[ c_p T^o \dot{B} + w \left( c_p \frac{\partial T}{\partial z} + g \right) \right] \left[ 1 - e^{-\epsilon(h-b)} \right] \frac{\pi}{\epsilon} \rho_b^o a^2 \end{aligned} \quad (\text{A20})$$

where (as in eq. (2b)) the dependence of  $\rho$  on  $B$  has been neglected.

Substituting the supercell parameters from table I gives

$$\dot{Q}(t) = 2.92 \times 10^4 w(t) a^2(t) \quad (\text{A21})$$

where the  $\dot{B}$  term (which contributes less than 1 percent for the supercell solution) has also been neglected. Because equation (A21) is independent of  $\dot{B}$ , this formula may be interpreted as

the diabatic heating required to maintain *neutral* buoyancy in the core. The additional heating required to give the buoyancy shown in figure 3(c) is negligible by comparison.

The corresponding moisture influx  $\dot{M}_v$  (in  $\text{g-s}^{-1}$ ) is given by dividing by the latent heat of condensation  $L_c$

$$\dot{M}_v(t) = 11.7 w(t) a^2(t) \quad (\text{A22})$$

Results of equations (A21) and (A22) give, respectively, the (temperature lapse modified) rate that heat or water vapor must be supplied to the core in order to support the inertial oscillation of the supercell solution.

## Appendix B

### Physical Interpretation of Translation Formulas

With the horizontal derivatives of the inner pressure (eqs. (10a) and (10b)), we may combine equations (8a) and (8b) into a single vector equation

$$\begin{aligned} & \frac{D}{2} (\mathbf{V}_b - \dot{\mathbf{r}}_c) + \frac{\zeta}{2} \hat{\mathbf{z}} \times (\mathbf{V}_b - \dot{\mathbf{r}}_c) + \boldsymbol{\omega} \times \hat{\mathbf{z}} w \\ & = -\frac{\nabla_{HP}}{\rho} - 2\boldsymbol{\Omega} \times \hat{\mathbf{z}} w - 2\Omega_z \hat{\mathbf{z}} \times \mathbf{V}_b \end{aligned} \quad (\text{B1})$$

where carats over the symbols denote unit vectors and

$$\begin{aligned} \mathbf{V}_b & \equiv (U_b, V_b, 0) \\ \dot{\mathbf{r}}_c & \equiv (\dot{x}_c, \dot{y}_c, 0) \\ \frac{\nabla_{HP}}{\rho} & = \frac{\Omega_y}{\epsilon} (-D, \zeta, 0) \end{aligned} \quad (\text{B2})$$

This result can be interpreted physically by considering an air parcel in the core and comparing equation (B1) with the momentum equation (5). The first term in equation (B1) represents the horizontal acceleration of the parcel resulting from translation of the divergence relative to the constant flow  $\mathbf{V}_b$ . (Recall that the reference level (here taken to be  $b$ ) can be any level in the middle layer, as mentioned in section 3.1.) The second term is interpreted similarly for relative translation of the vortex. The third term represents the horizontal acceleration of the parcel resulting from its upward motion amid vertical wind shear. (As mentioned in section 4.7, this term contributes to the right turn of the track during the intense phase when  $w$ ,  $D$ , and  $\xi$  all change signs.) These accelerations of the parcel are balanced on the right-hand side of equation (B1) by the force per unit mass resulting from the horizontal pressure gradient (eq. (B2)) and from the Coriolis force on the updraft and constant flow.

## Appendix C

### Further Properties of Inertial Oscillation

#### C1. Effect of Varying Peak Rossby Number

We will see how the waveforms for  $\zeta(t)$  and  $D(t)$  change as the (peak) initial value  $\zeta(0)$  varies from very small to large positive values (relative to  $\Omega_z = 4.77 \times 10^{-5} \text{ s}^{-1}$ ), with  $D(0) = 0$ . The corresponding peak Rossby number is given by  $\text{Ro}(0) = \zeta(0)/(2\Omega_z)$ . For the supercell solution,  $\text{Ro}(0) = 3.14$ , and the corresponding waveforms for  $\zeta(t)$  and  $D(t)$  are given in figures 3(a) and (b). These waveforms are explained physically (in section 5.2) by the inertial motion of parcels on the periphery of the core, as shown in figures 6(c) and (d).

For  $\text{Ro}(0) \ll 1$ , the nonlinear terms in the differential equations (8e) and (8f) can be neglected, and the waveforms are given by the simple harmonic expressions

$$\left. \begin{aligned} \zeta(t) &= \zeta(0) \cos 2\Omega_z t \\ D(t) &= \zeta(0) \sin 2\Omega_z t \end{aligned} \right\} \quad (\text{C1})$$

which have the same inertial period  $\pi/\Omega_z$  as the nonlinear solution. Comparing equations (C1) with the waveforms in figures 3(a) and (b) shows that as  $\text{Ro}(0)$  increases, the period divides into a quiescent phase and a rapidly varying intense phase.

The waveforms for a large Rossby number  $\text{Ro}(0) = 31.4$  are plotted in figures 7(a)–(e). (The corresponding peak temperature excess in the core is 1.06 K, which is reasonable for an updraft.) We see that as the peak Rossby number  $\text{Ro}(0)$  becomes large, the intense phase of the cycle  $\zeta(t) > 0$  becomes short. (In fact, the duration of the intense phase is roughly proportional to  $[\text{Ro}(0)]^{-1/2}$ .) This relationship, figures 7(a)–(e), and the corresponding inertial motion shown in figure 6(e) demonstrate the ability of the Coriolis force (in concert with the buoyant force) to generate high Rossby number flows of rapid growth and short duration.

#### C2. Inertial Oscillation of Anticyclonic Rotating Draft

The numerical solutions for  $\zeta(t)$  and  $D(t)$  presented in figures 3(a) and (b) represent a nonlinear inertial oscillation about the values  $\zeta = 0$ ,  $D = 0$  in the domain  $-2\Omega_z < \zeta(t) < \infty$ ,  $-\infty < D(t) < \infty$ . However, the oscillatory equations (8e) and (8f) remain unchanged by the substitution  $\zeta' = -\zeta - 4\Omega_z$ ,  $D' = D$ . Hence, a similar oscillation also exists about the values  $\zeta = -4\Omega_z$ ,  $D = 0$  in the domain  $-\infty < \zeta(t) < -2\Omega_z$ ,  $-\infty < D(t) < \infty$ . This second domain may be applicable to an anticyclonic supercell, as explained physically in section 5.5 and shown in figures 8 and 6(f). The corresponding curves for  $D(t)$ ,  $B(t)$ , and  $a(t)$  are the same as in figures 3(b)–(d); however, for otherwise similar initial conditions, the track of the anticyclonic rotating draft turns to the left, in agreement with observation (ref. 3).

### C3. Steady-State, Anticyclonic Vortex

The inner equations (4), (8e), (8f), (9), (A3), (A11), and (A20) also admit a steady-state solution given by

$$\left. \begin{aligned} \zeta &= -4\Omega_z \\ \dot{\theta} &= -2\Omega_z \\ \dot{x}_c &= \frac{2}{\epsilon}\Omega_y \\ D = w = \dot{y}_c = B = \dot{Q} &= 0 \end{aligned} \right\} \quad (\text{C2})$$

and  $a$ ,  $\xi$ ,  $\eta$ ,  $U_b$ , and  $V_b$  are arbitrary constants. The corresponding inertial motion is shown in figure 6(g) except that  $\nabla_H p$  is given by equations (10a) and (10b).

The translation of this anticyclonic vortex is due eastward, with a maximum speed of about  $1 \text{ m-s}^{-1}$  occurring at the equator. The arbitrary constants could, in principle, be determined by matching this inner solution to the environmental flow. No *cyclonic* steady-state solution of the inner equations exists. Even the null solution,  $\xi(t) = D(t) = 0$ , could be excluded because, by equations (9a) and (9b), the translational velocity components  $\dot{x}_c(t)$  and  $\dot{y}_c(t)$  become unbounded unless  $U_b = V_b = 0$  also.

## References

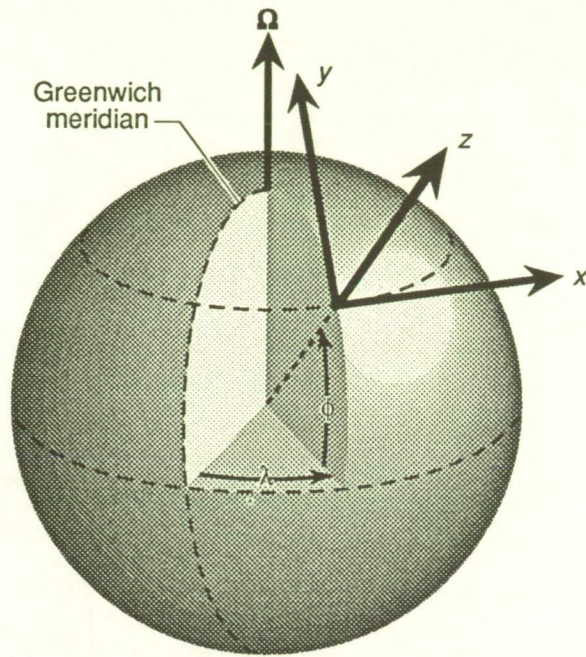
1. Holton, James R.: *An Introduction to Dynamic Meteorology*, Second ed. Academic Press, Inc., c.1979.
2. Newton, Chester W.; and Newton, Harriet Rodebush: Dynamical Interactions Between Large Convective Clouds and Environment With Vertical Shear. *J. Meteorol.*, vol. 16, no. 5, Oct. 1959, pp. 483-496.
3. Fujita, Tetsuya; and Grandoso, Hector: Split of a Thunderstorm Into Anticyclonic and Cyclonic Storms and Their Motion as Determined From Numerical Model Experiments. *J. Atmos. Sci.*, vol. 25, no. 3, May 1968, pp. 416-439.
4. Kuo, H. L.: Motions of Vortices and Circulating Cylinder in Shear Flow With Friction. *J. Atmos. Sci.*, vol. 26, no. 3, May 1969, pp. 390-398.
5. Raymond, David J.: A Model for Predicting the Movement of Continuously Propagating Convective Storms. *J. Atmos. Sci.*, vol. 32, no. 7, July 1975, pp. 1308-1317.
6. Moncrieff, M. W.: The Dynamical Structure of Two-Dimensional Steady Convection in Constant Vertical Shear. *Q. J. Royal Meteorol. Soc.*, vol. 104, no. 441, July 1978, pp. 543-567.
7. Bengtsson L.; and Lighthill, J., eds.: *Intense Atmospheric Vortices*. Springer-Verlag, 1982.
8. Lilly, Douglas K.: The Structure, Energetics and Propagation of Rotating Convective Storms. Part II: Helicity and Storm Stabilization. *J. Atmos. Sci.*, vol. 43, no. 2, Jan. 15, 1986, pp. 126-140.
9. Klemp, Joseph B.; and Wilhelmson, Robert B.: Simulations of Right- and Left-Moving Storms Produced Through Storm Splitting. *J. Atmos. Sci.*, vol. 35, no. 6, June 1978, pp. 1097-1110.
10. Schlesinger, Robert E.: A Three-Dimensional Numerical Model of an Isolated Deep Thunderstorm. Part II: Dynamics of Updraft Splitting and Mesovortex Couplet Evolution. *J. Atmos. Sci.*, vol. 37, no. 2, Feb. 1980, pp. 395-420.
11. Rotunno, Richard; and Klemp, Joseph B.: The Influence of the Shear-Induced Pressure Gradient on Thunderstorm Motion. *Mon. Weather Review*, vol. 110, no. 2, Feb. 1982, pp. 136-151.
12. Klemp, Joseph B.: Dynamics of Tornadic Thunderstorms. *Annual Review of Fluid Mechanics*, Volume 19, John L. Lumley, Milton Van Dyke, and Helen L. Reed, eds., Annual Reviews Inc., 1987, pp. 369-402.
13. Kessler, Edwin, ed.: *Thunderstorm Morphology and Dynamics*, Second ed., Revised and Enlarged. Volume 2 of *Thunderstorms: A Social, Scientific, and Technological Documentary*. Univ. of Oklahoma Press, c.1986.
14. Costen, R. C.; and Stock, L. V.: Supercells and Downbursts as Possible Manifestations of a Nonlinear Oscillation. *Suppl. to EOS Trans.*, American Geophys. Union, Apr. 23, 1991, p. 72.
15. Haltiner, George J.; and Martin, Frank L.: *Dynamical and Physical Meteorology*. McGraw-Hill Book Co., 1957.
16. Miller, L. Jay; Tuttle, John D.; and Knight, Charles A.: Airflow and Hail Growth in a Severe Northern High Plains Supercell. *J. Atmos. Sci.*, vol. 45, no. 4, Feb. 15, 1988, pp. 736-762.
17. Menke, William; and Abbott, Dallas: *Geophysical Theory*. Columbia Univ. Press, c.1990.
18. Howarth, L., ed.: *Modern Developments in Fluid Dynamics—High Speed Flow*, Volume I. Oxford Univ. Press, 1953.
19. Spiegel, Murray R.: *Schaum's Outline of Theory and Problems of Advanced Calculus*. McGraw-Hill, Inc., c.1963.
20. Urabe, Minoru: *Nonlinear Autonomous Oscillations*. Academic Press, 1967.
21. Foote, G. B.; and Fankhauser, J. C.: Airflow and Moisture Budget Beneath a Northeast Colorado Hailstorm. *J. Appl. Meteorol.*, vol. 12, no. 8, Dec. 1973, pp. 1330-1353.
22. Phillips, Byron B.: Precipitation Characteristics of a Sheared, Moderate Intensity, Supercell-Type Colorado Thunderstorm. *J. Appl. Meteorol.*, vol. 12, no. 8, Dec. 1973, pp. 1354-1363.
23. Musil, D. J.; Sand, W. R.; and Schleusener, R. A.: Analysis of Data From T-28 Aircraft Penetrations of a Colorado Hailstorm. *J. Appl. Meteorol.*, vol. 12, no. 8, Dec. 1973, pp. 1364-1370.
24. Bushnell, R. H.: Dropsonde Measurements of Vertical Winds in the Colorado Thunderstorm of 22 July 1972. *J. Appl. Meteorol.*, vol. 12, no. 8, Dec. 1973, pp. 1371-1374.
25. Barnes, Stanley L.: Some Aspects of a Severe, Right-Moving Thunderstorm Deduced From Mesonet Rawinsonde Observations. *J. Atmos. Sci.*, vol. 27, no. 4, July 1970, pp. 634-648.

Table I. Initial Values and Parameters Used in Supercell Solution

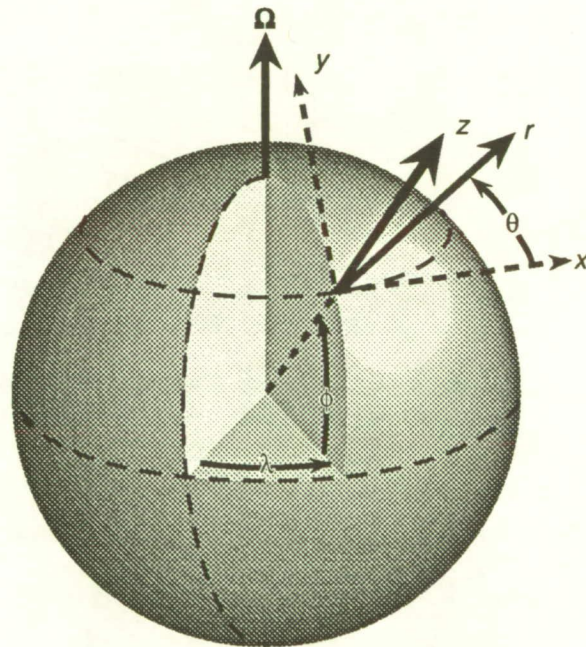
$D(0), \text{s}^{-1}$	0
$\xi(0), \text{s}^{-1}$	$-1.74 \times 10^{-4}$
$\eta(0), \text{s}^{-1}$	$9.85 \times 10^{-4}$
$\zeta(0), \text{s}^{-1}$	$3.0 \times 10^{-4}$
$w(0), \text{m-s}^{-1}$	0
$a(0), \text{km}$	13.8
$\theta(0), \text{rad}$	0
$x_c(0), \text{m}$	0
$y_c(0), \text{m}$	0
$U_b, \text{m-s}^{-1}$	8.33
$V_b, \text{m-s}^{-1}$	1.42
$\Omega_y, \text{s}^{-1}$	$5.49 \times 10^{-5}$
$\Omega_z, \text{s}^{-1}$	$4.77 \times 10^{-5}$
$\epsilon \text{ m}^{-1}$	$1.25 \times 10^{-4}$
$b, \text{km}$	4.43
$h, \text{km}$	8.0
$\rho_b^o, \text{kg-m}^{-3}$	0.77
$p(b), \text{kPa}$	60.5
$T(b), \text{K}$	273
$T(h), \text{K}$	253
$\partial T / \partial z, \text{K-m}^{-1}$	$-5.6 \times 10^{-3}$
$T^o, \text{K}$	273

Table II. Computational Time and Mountain Daylight Time for Supercell Solution

Description	$t, \text{ks}$	MDT
Middle of quiescent phase, maximum core diameter	32.9	0653
Intermediate quiescent phase	44.6	1008
End of quiescent phase, beginning of intense phase, zero rotation	56.3	1323
Maximum horizontal convergence, maximum downdraft speed, zero buoyancy	60.9	1439
Intermediate intense phase	63.6	1523
Middle of intense phase, minimum core diameter, maximum rotation rate, transition point for $w$ , turning point of path	65.9	1602
Intermediate intense phase	68.2	1641
Maximum horizontal divergence, maximum updraft speed, zero buoyancy	70.9	1725
End of intense phase, beginning of quiescent phase, zero rotation	75.5	1841
Intermediate quiescent phase	87.2	2156
Middle of quiescent phase, maximum core diameter	98.9	0111



(a) Cartesian frame  $x, y, z$ .



(b) Alternative cylindrical frame  $r, \theta, z$ .

Figure 1. Local tangential coordinate frame whose origin is fixed at point on surface of Earth (mean sea level) of latitude  $\phi$  and east longitude  $\lambda$ .

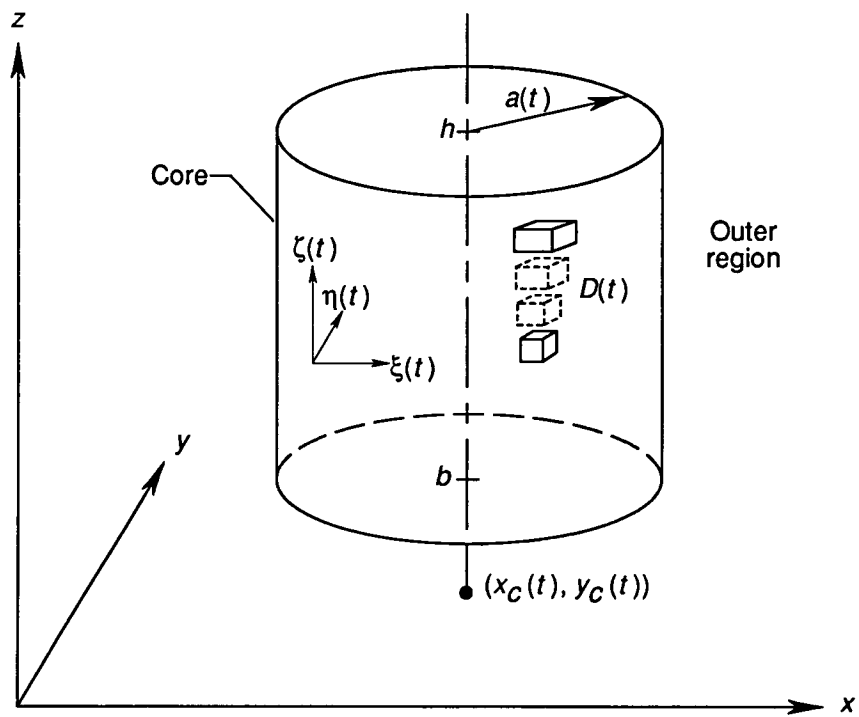
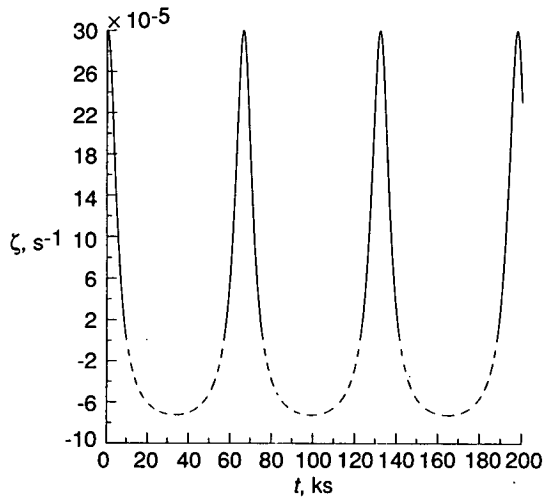
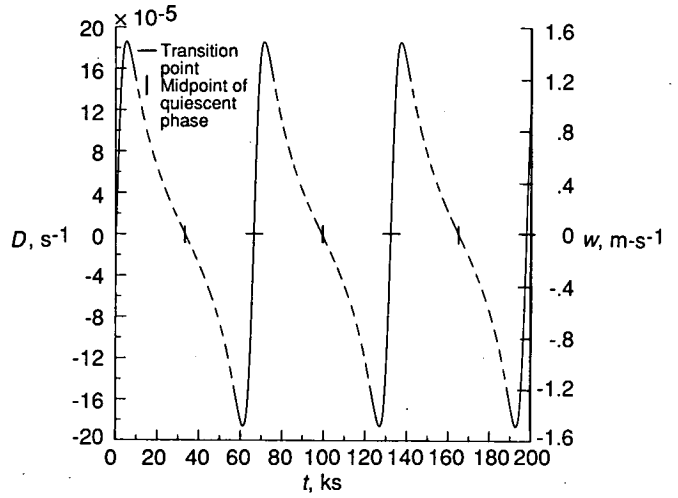


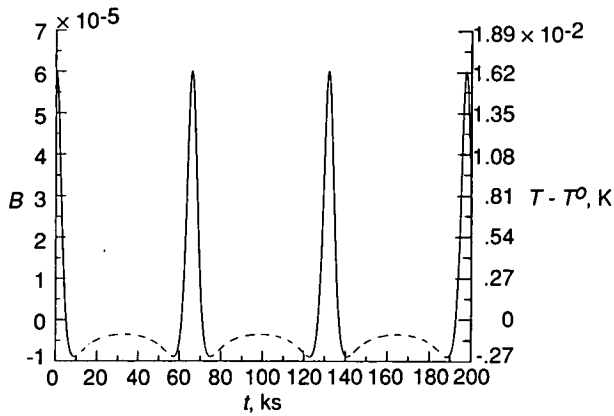
Figure 2. Idealized vertical rotating draft with core of radius  $a(t)$  between heights  $b$  and  $h$ .



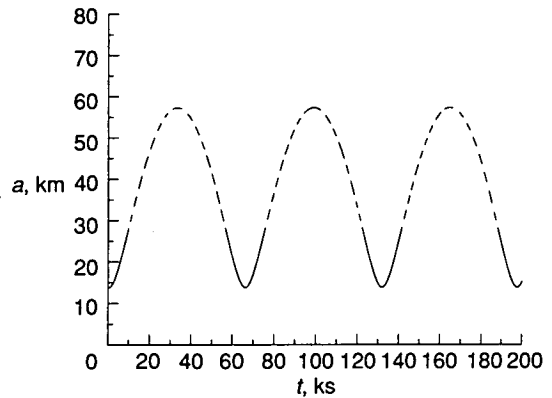
(a) Vertical component of vorticity  $\zeta$  against time  $t$ .



(b) Divergence  $D$  and draft velocity  $w$  against  $t$ .

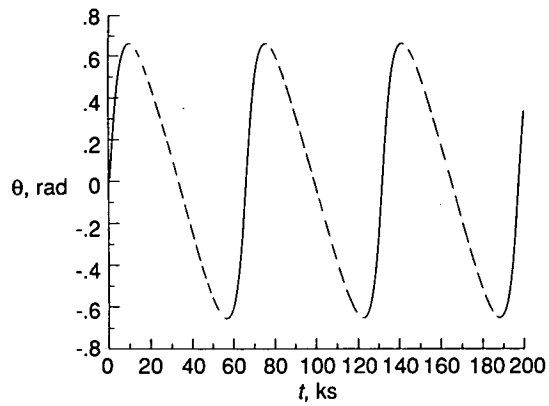


(c) Core buoyancy  $B$  (normalized density deficit) and corresponding temperature excess  $T - T^0$  against  $t$ .

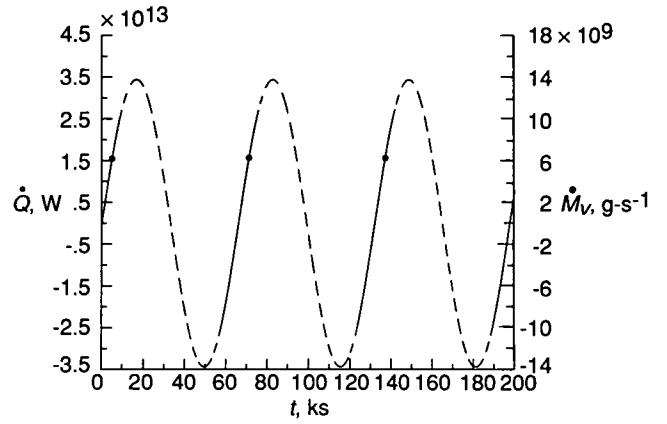


(d) Core radius  $a$  against  $t$ .

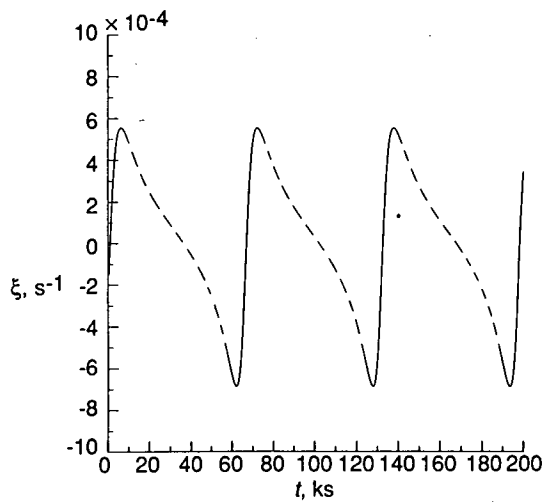
Figure 3. Supercell inner solution of equations (4), (8c)–(8f), (9), (A3), (A11), and (A21) for initial values and parameters given in table I. The intense phase of each cycle is indicated by a solid line, and quiescent phase by a broken line.



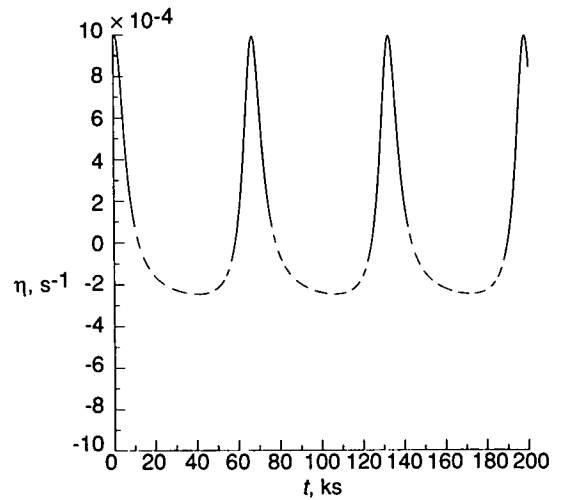
(e) Angular displacement of core fluid  $\theta$  against  $t$ .



(f) Total diabatic core heating  $\dot{Q}$  and corresponding water vapor influx  $\dot{M}_v$  against  $t$ .

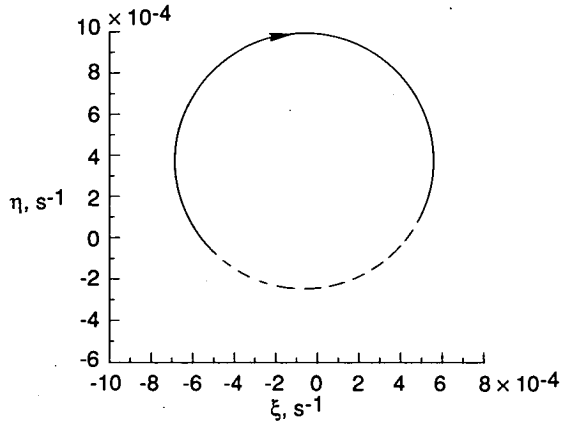


(g)  $x$  component of vorticity  $\xi$  against  $t$ .

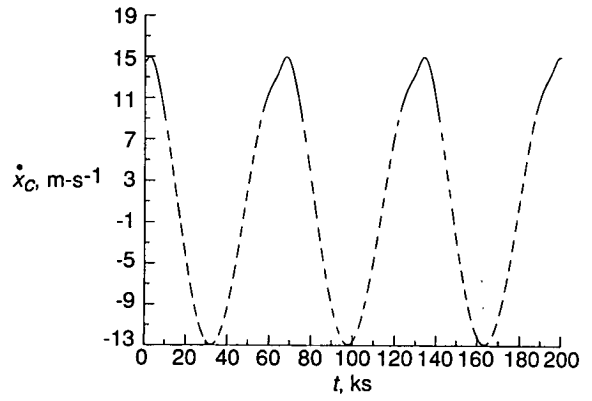


(h)  $y$  component of vorticity  $\eta$  against  $t$ .

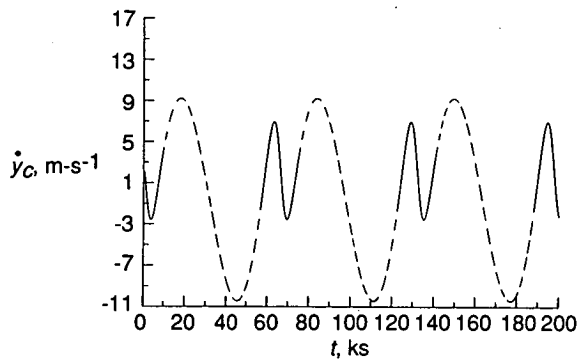
Figure 3. Continued.



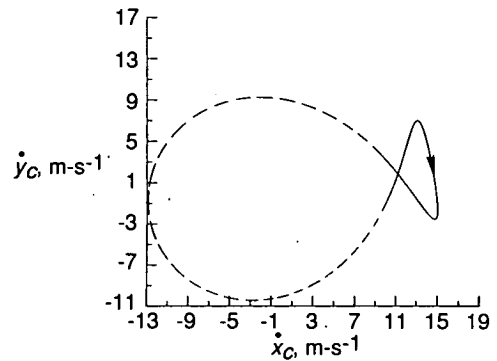
(i) Phase diagram on  $\xi$ - $\eta$  plane with arrow indicating anticyclonic rotation of horizontal vorticity vector and located in middle of intense phase.



(j)  $x$  component of translation  $\dot{x}_c$  against  $t$ .

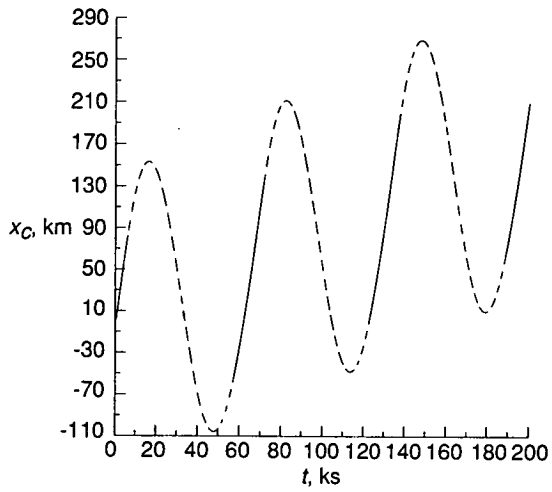


(k)  $y$  component of translation  $\dot{y}_c$  against  $t$ .

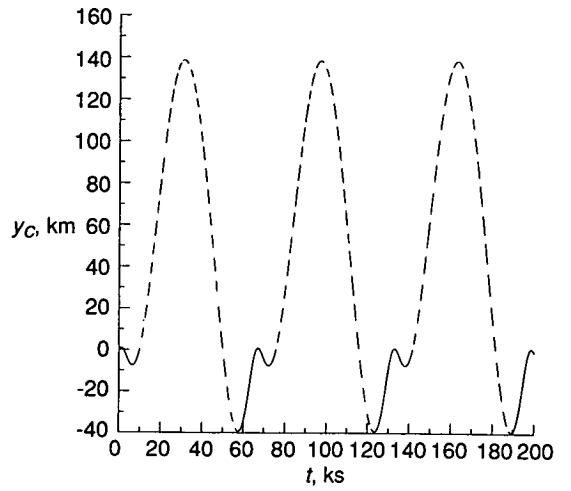


(l) Phase diagram on  $\dot{x}_c$ - $\dot{y}_c$  plane with arrow indicating sense of traversal and located in middle of intense phase.

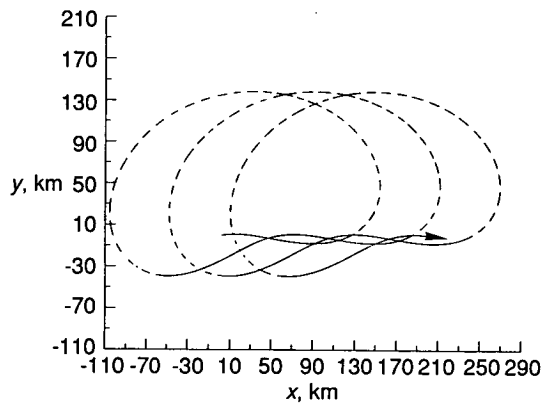
Figure 3. Continued.



(m)  $x$  coordinate of rotating draft centerline  $x_c$  against  $t$ .

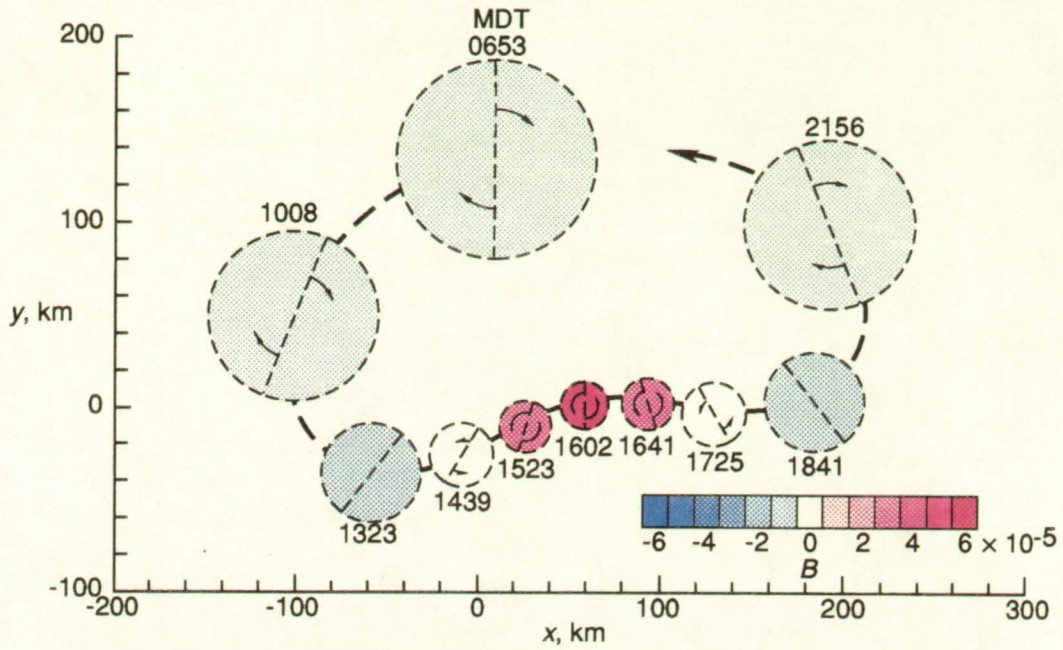


(n)  $y$  coordinate of rotating draft centerline  $y_c$  against  $t$ .

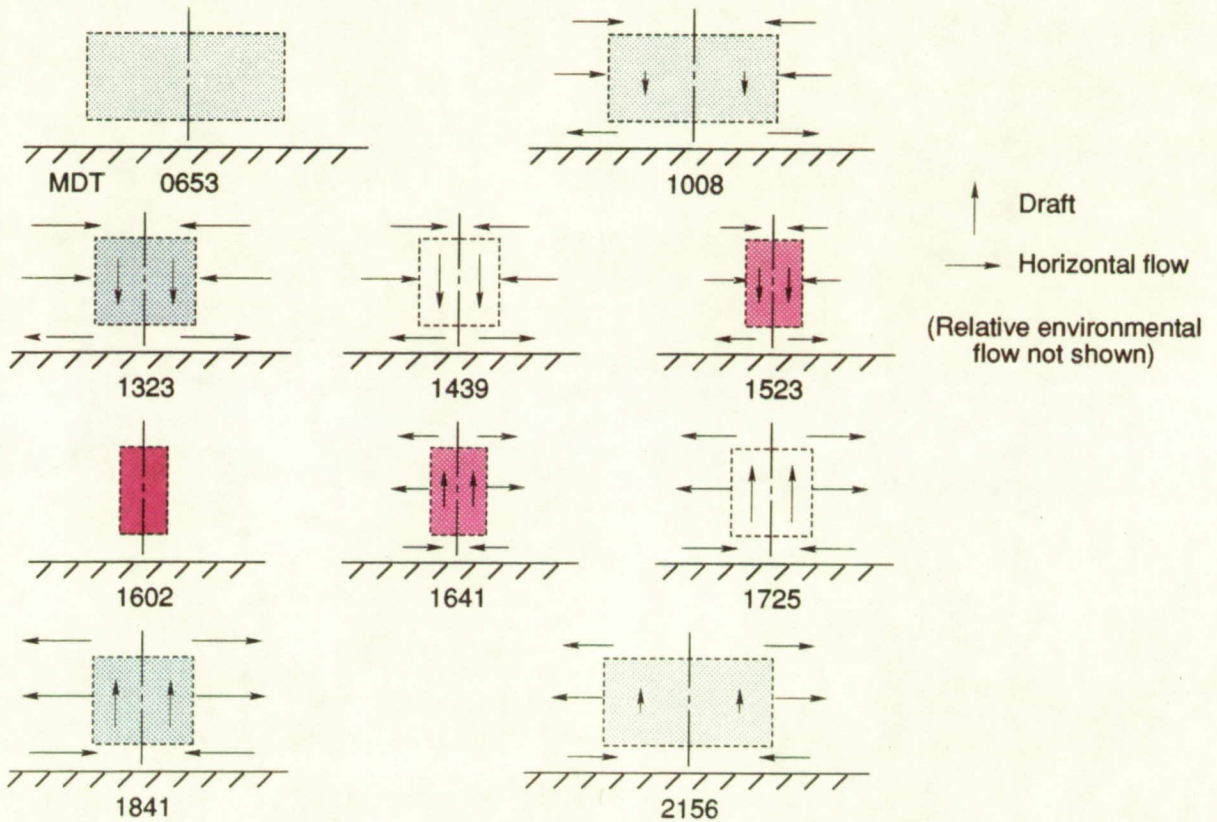


(o) Track of rotating draft centerline on horizontal  $x$ - $y$  plane.

Figure 3. Concluded.



(a) Aerial view. Angles of diameter lines indicate angular displacement of core fluid (fig. 3(e)). See radar data in figure 5.



(b) Side view with vertical dimension exaggerated.

Figure 4. Core sequence of vertical rotating draft for supercell solution.

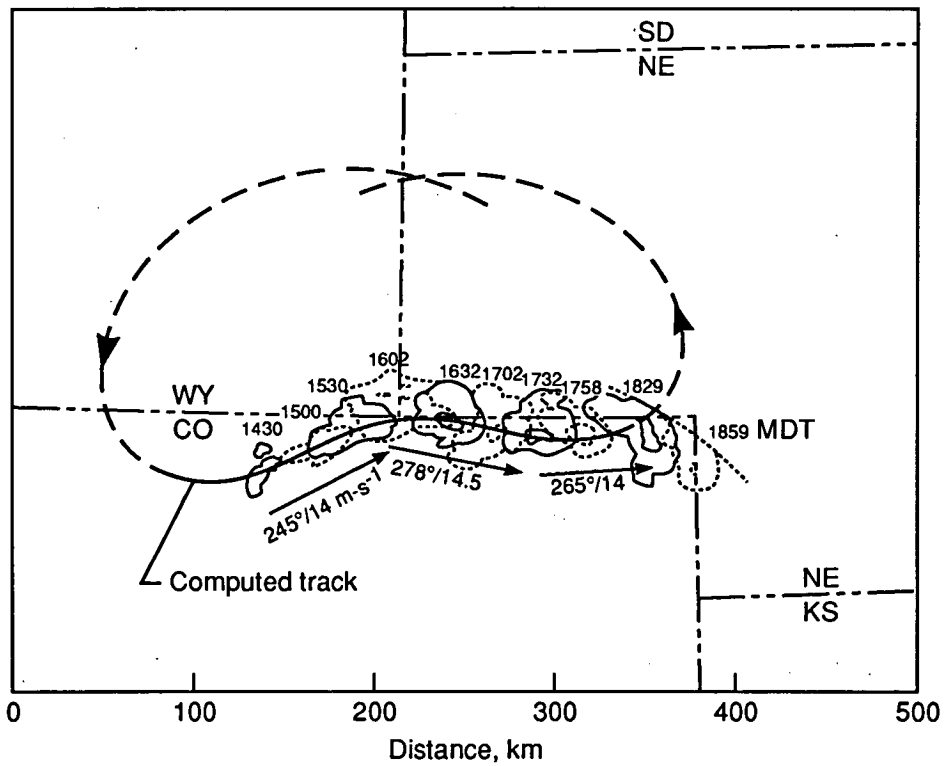
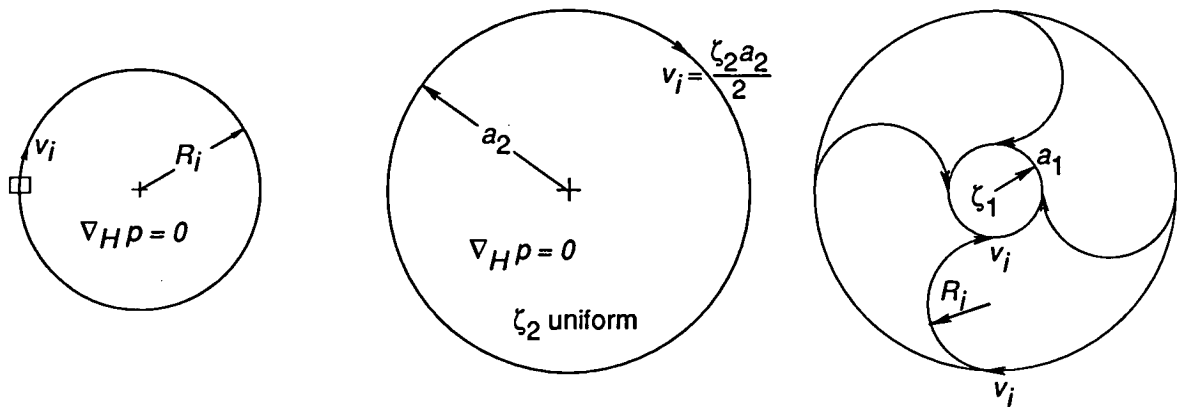


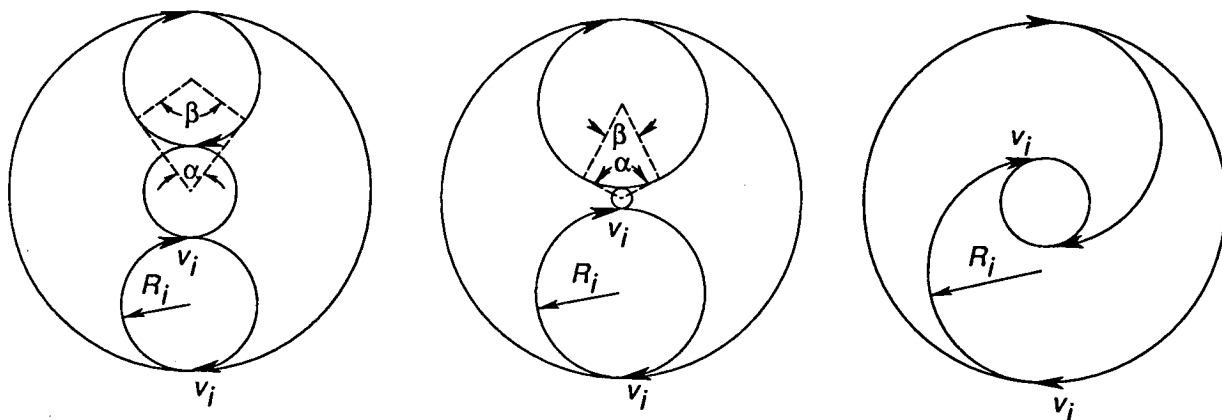
Figure 5. Radar echoes obtained at 30-min intervals from documented supercell. Adapted from reference 21 with permission of the American Meteorological Society.



(a) Horizontal, frictionless, inertial motion of fluid parcel with speed  $v_i$ .

(b) Basic rotating draft that oscillates in place (appendix A) when its core radius  $a_2 = 57.3$  km is at its maximum.

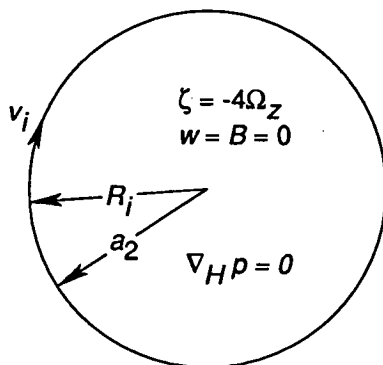
(c) Cyclonic spin-up resulting from the inward track of inertial parcels on the core periphery.



(d) Complete inertial cycle.

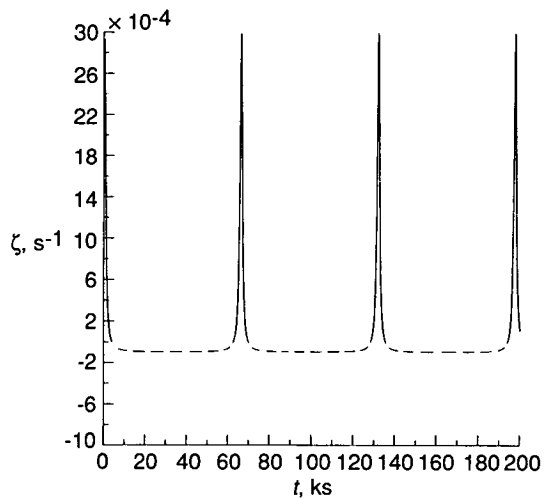
(e) Higher cyclonic spin-up.

(f) Anticyclonic spin-up.

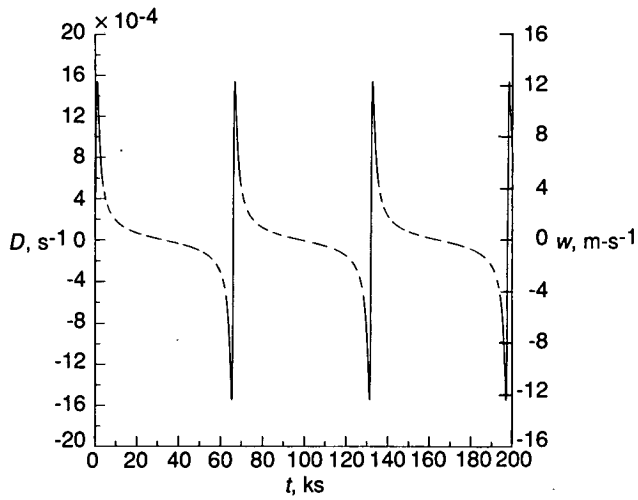


(g) Steady-state anticyclonic Rankine vortex corresponding to solution given in section C3.

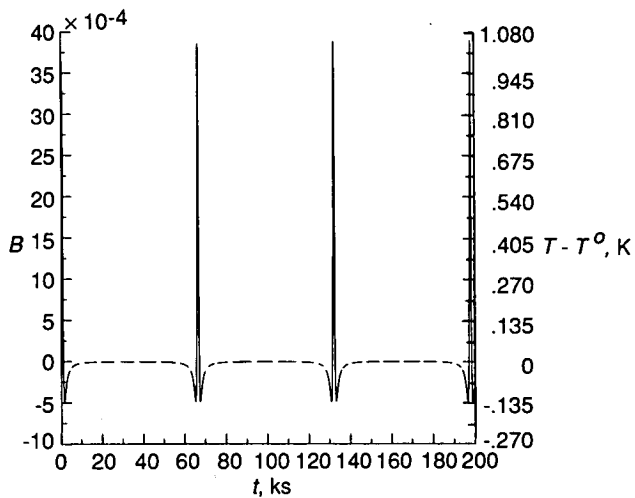
Figure 6. Physics of inertial oscillation of vertical rotating draft, as viewed from above.



(a)  $\zeta$  against  $t$ .

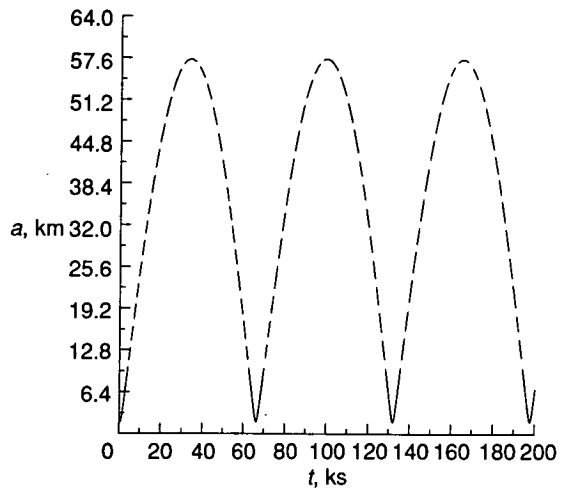


(b)  $D$  and  $w$  against  $t$ .

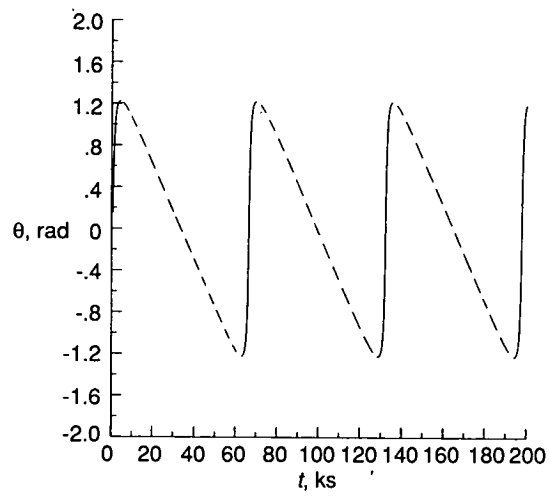


(c)  $B$  and  $T - T^0$  against  $t$ .

Figure 7. Solutions of equations (4), (8e), (8f), (A3), and (A11) for high initial Rossby number  $Ro(0) = \zeta(0)/2\Omega_z = 31.4$ , where  $D(0) = 0$  and  $\Omega_z = 4.77 \times 10^{-5} \text{ s}^{-1}$ . (Also see fig. 6(e).)



(d)  $a$  against  $t$ .



(e)  $\theta$  against  $t$ .

Figure 7. Concluded.

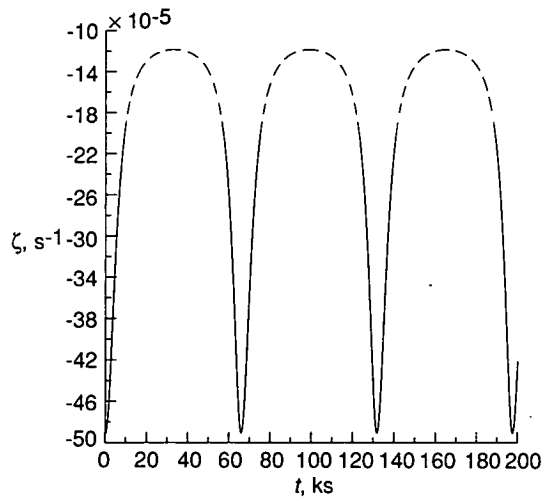
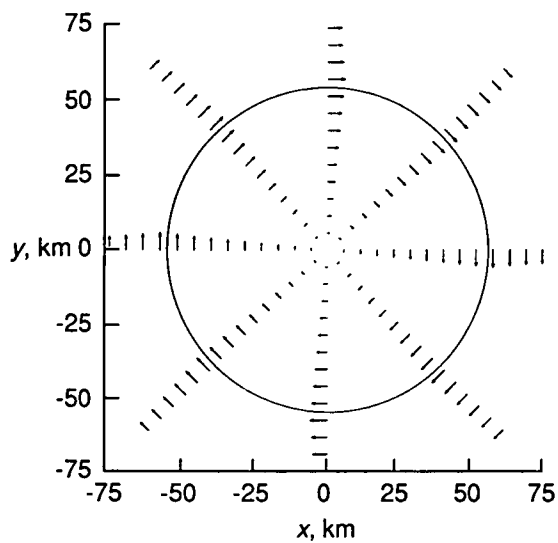
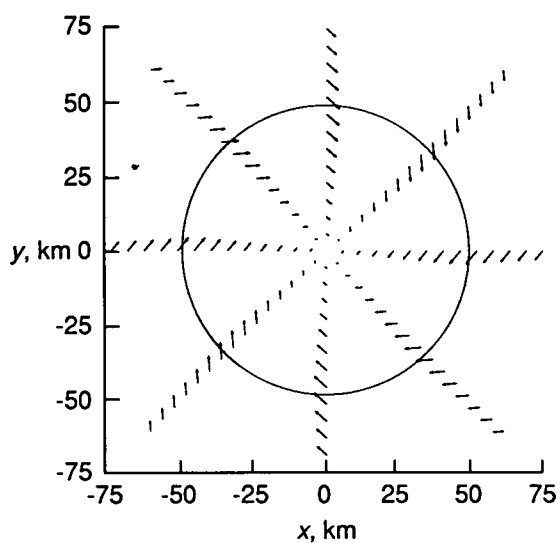


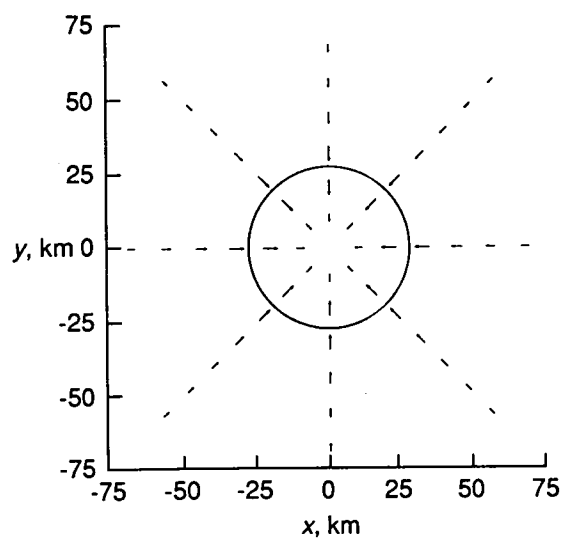
Figure 8.  $\zeta$  for anticyclonic vertical rotating draft. (Also see fig. 6(f).)



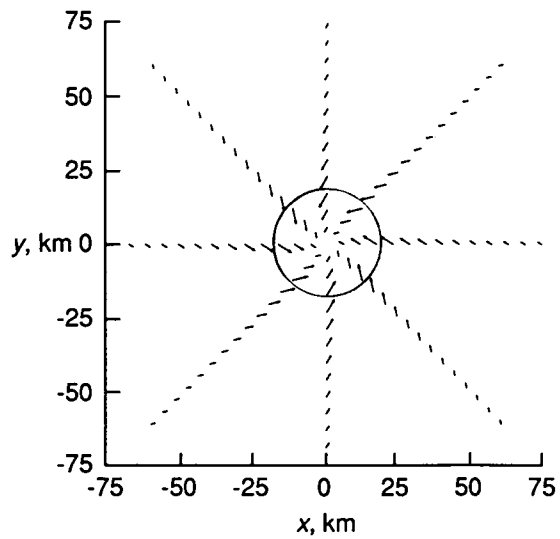
(a)  $t = 32.9$  ks.



(b)  $t = 44.6$  ks.

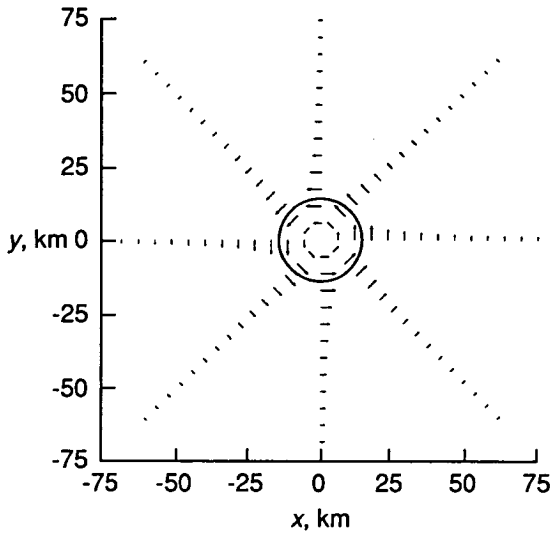


(c)  $t = 56.3$  ks.

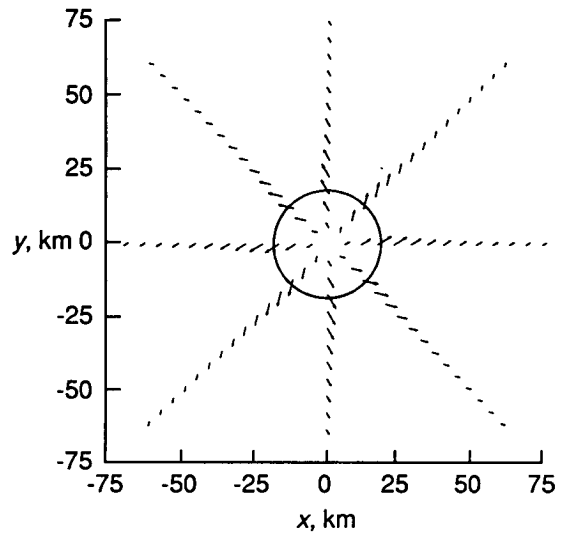


(d)  $t = 60.9$  ks.

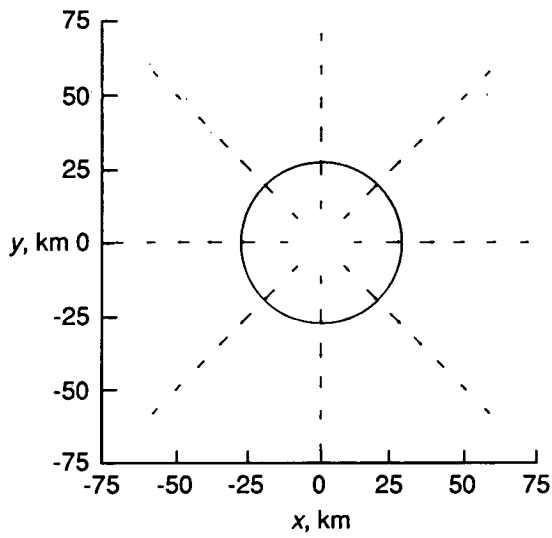
Figure 9. Horizontal flow field sequence for the basic rotating draft that oscillates in place (appendix A).



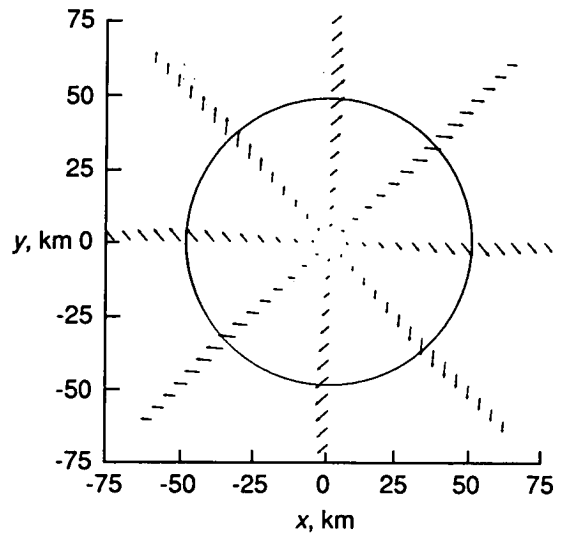
(e)  $t = 65.9$  ks.



(f)  $t = 70.9$  ks.



(g)  $t = 75.5$  ks.



(h)  $t = 87.2$  ks (cycle complete at  $t = 98.9$  ks).

Figure 9. Concluded.

A video supplement L-0592-97 is available for purchase.

In this video (8 min., color, sound, VHS), animation depicts the inertial oscillation of a new mathematical model ("vertical rotating draft") for spinning up a single supercell storm. The oscillation consists of a long quiescent phase when the draft is large in diameter and rotates anticyclonically and a short intense phase when the draft is small and cyclonic. During the intense phase, the rotating draft resembles a supercell. The physical basis for the oscillation is depicted by tracking air parcels in the draft as they move along inertial circles (projected on a horizontal plane), where the horizontal pressure gradient is zero and the Coriolis force balances the centrifugal force. A side view of the oscillation shows that contraction and expansion are linked, respectively, to buoyantly driven compressible downdraft and updraft. An aerial view tracks the draft as it moves above the surface of the Earth and turns to the right during the intense phase. Radar echoes from a supercell storm are superimposed for comparison. The data appear to support only the intense phase. A critical experiment would measure the predominantly downward flow that theoretically occurs before the right turn in a supercell track and causes contraction and spin-up.

Requests for the video should be addressed to

ATTN USER SERVICES  
NASA CENTER FOR AEROSPACE INFORMATION  
PO BOX 8757  
BALTIMORE MD 21240-0757

Cut here ✂ -----

Please send \_\_\_\_\_ copies of video supplement L-0592-97 to NASA TP-3230.

Attn: \_\_\_\_\_

Name

\_\_\_\_\_

Title

\_\_\_\_\_

Organization

\_\_\_\_\_

Street address

\_\_\_\_\_

City and State

\_\_\_\_\_

Zip code

# REPORT DOCUMENTATION PAGE

*Form Approved*  
*OMB No. 0704-0188*

Public reporting burden for this collection of information is estimated to average 1 hour per response, including the time for reviewing instructions, searching existing data sources, gathering and maintaining the data needed, and completing and reviewing the collection of information. Send comments regarding this burden estimate or any other aspect of this collection of information, including suggestions for reducing this burden, to Washington Headquarters Services, Directorate for Information Operations and Reports, 1215 Jefferson Davis Highway, Suite 1204, Arlington, VA 22202-4302, and to the Office of Management and Budget, Paperwork Reduction Project (0704-0188), Washington, DC 20503.

<b>1. AGENCY USE ONLY</b> <i>(Leave blank)</i>	<b>2. REPORT DATE</b> September 1992	<b>3. REPORT TYPE AND DATES COVERED</b> Technical Paper	
<b>4. TITLE AND SUBTITLE</b> Inertial Oscillation of a Vertical Rotating Draft With Application to a Supercell Storm		<b>5. FUNDING NUMBERS</b> WU 506-41-41-01	
<b>6. AUTHOR(S)</b> Robert C. Costen and Larry V. Stock			
<b>7. PERFORMING ORGANIZATION NAME(S) AND ADDRESS(ES)</b> NASA Langley Research Center Hampton, VA 23681-0001		<b>8. PERFORMING ORGANIZATION REPORT NUMBER</b> L-16987	
<b>9. SPONSORING/MONITORING AGENCY NAME(S) AND ADDRESS(ES)</b> National Aeronautics and Space Administration Washington, DC 20546-0001		<b>10. SPONSORING/MONITORING AGENCY REPORT NUMBER</b> NASA TP-3230	
<b>11. SUPPLEMENTARY NOTES</b> Costen: Langley Research Center, Hampton, Virginia; Stock: Hampton University, Hampton, Virginia. Video supplement L-0592-97 available for purchase on request.			
<b>12a. DISTRIBUTION/AVAILABILITY STATEMENT</b>  Unclassified-Unlimited  Subject Category 47		<b>12b. DISTRIBUTION CODE</b>	
<b>13. ABSTRACT</b> <i>(Maximum 200 words)</i> An analytic model ( <sup>a</sup> vertical rotating draft <sup>b</sup> ), which includes the gross features of a supercell storm on an <i>f</i> -plane, undergoes an inertial oscillation that appears to have been overlooked in previous analytic and numerical models. The oscillation is nonlinear and consists of a long quiescent phase and a short intense phase. During the intense phase, the rotating draft has the following features of a supercell: the diameter of the core contracts as it spins up and expands as it spins down; if vertical wind shear is included, the track of the rotating draft turns to the right (an anticyclonic rotating draft turns to the left); this turning point is followed by a predominantly upward flow; and the horizontal pressure gradient is very small (a property of most tornadoless supercells). The rapid spin-up during the intense phase and the high Rossby numbers obtainable establish the ability of the Coriolis force to spin up single cyclonic or anticyclonic supercells by means of this inertial oscillation. This surprising result has implications for numerical supercell simulations, which generally do not rely on the Coriolis force as a source of rotation. The physics and mathematics of the inertial oscillation are given, and the solution is applied to a documented supercell.			
<b>14. SUBJECT TERMS</b> Supercell thunderstorm; Inertial oscillation		<b>15. NUMBER OF PAGES</b> 47	
		<b>16. PRICE CODE</b> A03	
<b>17. SECURITY CLASSIFICATION OF REPORT</b> Unclassified	<b>18. SECURITY CLASSIFICATION OF THIS PAGE</b> Unclassified	<b>19. SECURITY CLASSIFICATION OF ABSTRACT</b>	<b>20. LIMITATION OF ABSTRACT</b>